The Early Eocene equable climate problem: Can perturbations of climate model parameters identify possible solutions?

Journal:	*Philosophical Transactions A*
Manuscript ID:	RSTA-2013-0123
Article Type:	Research
Date Submitted by the Author:	04-Mar-2013

Complete List of Authors:	Sagoo, Navjit; University of Bristol, School of Geographical Sciences Valdes, Paul; University of Bristol, School of Geographical Sciences Flecker, Rachel; University of Bristol, School of Geographical Sciences Gregoire, Lauren; University of Bristol, School of Geographical Sciences

Issue Code: Click here to find the code for your issue.:	DM1011
Subject:	Climatology < EARTH SCIENCES
Keywords:	Perturbed physics ensemble, Eocene, Eocene Model, Equable, Data/Model

The Early Eocene equable climate problem: Can perturbations of climate model parameters identify possible solutions?

Navjit Sagoo, Paul Valdes, Rachel Flecker, Lauren Gregoire

School of Geographical Sciences, University of Bristol, University Road, Bristol, BS8 1SS, UK

1 Abstract

Geological data for the early Eocene (56 Ma to 47.8 Ma) indicates extensive global warming, with very warm temperatures at both poles. However, despite numerous attempts to simulate this warmth, there are remarkable data–model differences in the prediction of these polar surface temperatures, resulting in the so called "equable climate problem".

In this paper, for the first time an ensemble with a perturbed climate-sensitive model parameters approach has been applied to modelling the early Eocene climate. We performed more than 100 simulations with perturbed physics parameters, and identified two simulations which have an optimal fit with the proxy data. We have simulated the warmth of the early Eocene at 560 ppmv CO_2 which is a much lower CO_2 level than many other models. We investigate the changes in atmospheric circulation, cloud properties and ocean circulation that are common to these simulations and how they differ from the remaining simulations in order to understand what mechanisms contribute to the polar warming.

The parameter set from one of the optimal early Eocene simulations also produces a favourable fit for the Last Glacial Maximum boundary climate and outperforms the control parameter set for the present day. Although this does not "prove" that this model is correct, it is very encouraging that there is a parameter set that creates a climate model able to simulate well very different paleoclimates and the present day climate. Interestingly, to achieve the great warmth of the early Eocene this version of the model does not have a strong future climate change Charney climate sensitivity. It produces a Charney climate sensitivity of 2.7 ˚C whereas the mean value of the 18 models in the AR4 is

3.26 °C ± 0.69 °C. Thus this value is within the range and below the mean of the models included in the IPCC Fourth Assessment Report (AR4).

Key word index: Perturbed physics ensemble, Eocene, Eocene model, Equable, Data/model

2 Introduction

The term equable climate has been used to describe the global extent of warmth in past climates which have a reduced equator to pole temperature difference, warm polar regions with a reduced seasonality and ice free conditions at both poles [1,2]. The extent of this warming is supported by a wide range of data. Recent syntheses of terrestrial (Huber and Caballero, 2011) [3] and marine (Lunt et al 2012) [4] proxy climate data for the early Eocene suggest that the polar temperatures were 15 °C or more but that the tropics were only slightly warmer than modern. Moreover, palaeobotanical data also suggests that the high latitudes were above freezing throughout the year [5] which is a major change over present conditions despite the fact that the continents are not that different from the modern.

The early Eocene equable climate problem relates to differences between climate model simulations and proxy reconstructions of the early Eocene and the climate inferred from climate proxies. The modern generation of climate models has managed to capture much of this warmth from the proxy data in the low and mid latitudes by forcing the climate with very high concentrations of CO_2, 16 x pre-industrial concentrations of CO_2 (i.e. Huber & Caballero, 2011; Winguth et al., 2012) [3,6], but simulating above freezing temperatures at the poles all year round is difficult. The assumption of a strong seasonal bias in the proxy data must currently be assumed in order to reconcile proxy polar temperatures with climate model output [4].

Estimates of early Eocene temperatures include annual Sea Surface Temperatures (SSTs) of up to 27 °C [7] and terrestrial mean annual temperatures (MATs) of up to 18 °C [8] at palaeolatitudes >80°N. In the Southern Hemisphere SSTs between 17 °C and 32 °C [9–11] have been reconstructed at palaeolatitudes >60°S, while terrestrial MATs between 12 °C and 18.8 °C have been reconstructed at similar latitudes [12–14]. These high latitude temperatures are likely to have been sufficient to prevent any significant permanent ice cover. Whilst there is reasonable data coverage for the mid and high latitudes, data from the low latitudes are scarce. Tropical SST data are available from the Tanzania drilling project, this indicates SSTs at a paleolatitude of 18°S were ~33 ˚C [15]. One of the features inferred from this distribution of temperatures is that the temperature difference between the pole and the equator was much reduced compared to the modern day. There is also evidence of an enhanced hydrological cycle in the high latitudes during the early Eocene [16–18]. Water vapour has an impact on the radiation balance of the planet through the water vapour greenhouse effect, the cloud greenhouse effect and via reflection of shortwave radiation from clouds and ice [19]. Understanding what role an intensified hydrological cycle may play in developing and maintaining an equable climate is therefore also of interest.

The first paper on the early Eocene equable climate problem was published over thirty years ago [20] and substantial modelling efforts have been undertaken since then in order to simulate the early Eocene climate. Many advances in model development have also been made, and whereas the earliest Eocene models were limited to, either energy balance models (EBMs) or early general circulation models (GCMs) with fixed seasons, the current generation of models simulate the dynamics of the atmospheres and oceans and in some cases vegetation, are of higher resolution and have improved and revised physics. This has consequently improved our ability to simulate the Eocene climate. Meanwhile, advances in existing proxy methods, the development of new methods and the acquisition of additional proxy data have led to the warmer, revised temperatures for the tropical marine realm [21] and terrestrial realms at all latitudes [22–25]. Thus, the equable climate problem is still apparent in the proxy datasets. Whilst modelling studies have improved in their simulation of the early Eocene, the processes that contribute to the amplification of polar temperatures during the early Eocene are difficult to accurately model (e.g. clouds) and are not well understood. However the model-data discrepancy persists in the high latitudes. The aim of this paper is to understand whether perturbing uncertain climate model parameters can offer insight into the climate processes involved in developing and maintaining the equable early Eocene climate.

2.1 Previous Eocene modelling studies

Many of the earliest model experiments of the early Eocene, run with increased CO_2 concentrations compared to the modern, simulated high latitudes and continental interiors which were warmer than the modern, but not warm enough compared to the proxy climate evidence of the early Eocene. Sloan & Barron, (1990, 1992) [26,27] simulated high latitudes and continental interiors that are warmer than the modern, but still cooler than the proxy climate evidence. This model-data mismatch generated a range of possible explanations including missing components and processes in the models such as polar stratospheric clouds, [27,28]; and tropical cyclones [29–31] to approximations in the boundary conditions associated with coarse model resolution, like for example the presence of large lakes e.g. [32,33]; altered orbits e.g. [34]; and the role of heat transport [35,36].

A recurring theme in early Eocene modelling studies is the contribution of clouds in equable climates. Sloan et al., (1999); Kirk-Davidoff et al., (2002) and Kirk-Davidoff and Lamarque, (2007) [28,37,38] have all investigated the role of polar stratospheric clouds (PSCs) in equable climates in response to elevated concentrations of CO_2 and CH_4. Sloan et al., (1999) included idealised prescribed PSCs in the GCM Genesis version 2 which resulted in up to 20 °C warming in oceanic regions where sea ice was reduced. This warming was still insufficient to account for warming seen in the proxy data available at the time, but compared to more recent proxy data these simulations were ~10 °C too cool at latitudes of around 60°. Kirk-Davidoff et al., (2002) and Kirk-Davidoff and Lamarque, (2007), investigated the mechanisms that led to the formation of PSCs and the response of the climate, PSCs were found to warm in response to higher CO_2 via changes in stratospheric circulation and water content, but the large radiative effects required to warm the polar regions were found to be related to ice crystal number density in the PSCs, and a lack of theoretical knowledge may have prevented these hypotheses from being developed further.

Abbot & Tziperman, 1998 [39] identified a high latitude cloud radiative forcing feedback using a simple column model. They found that increased extra tropical surface temperatures led to the initiation of strong atmospheric convection, the convective clouds led to additional warming of the high latitudes. The radiative effect of the resulting convective clouds reduced the equator to pole temperature difference (EPTD) by 8-10 °C. Further work using this column model investigated the constraints atmospheric and oceanic heat transport and CO_2 concentration had on the convective cloud feedback [40]. This feedback was found to be present in modern model simulations forced with CO_2 = 2240 ppmv, and for the Eocene with CO_2 = 560 ppmv.

An alternative solution to the equable climate problem was suggested by Kump & Pollard, (2008) [41] and Kiehl et al., (this volume). Cloud condensation nuclei (CCN) play an important role in cloud properties such as cloud water content, cloud opacity and cloud lifetime. In the past, the distribution of CCN was likely different to today's because the distribution and composition of atmospheric aerosol was different [42]. Based on this, Kump & Pollard (2008) increased CCN radii in a Cretaceous climate simulation using the Genesis (version 3.0) GCM. This resulted in a decrease in cloud amount and cloud albedo leading to a dramatic warming, both globally and at the poles and a decrease in the EPTD.

Lunt et al., (2012) [4] have recently published a review on Eocene modelling termed EoMIP (the Eocene modelling intercomparison project) in which they compare five recent modelling studies for the early Eocene. The modelling studies have all been run with different objectives; different boundary conditions and multiple values of CO_2 have been used in some studies. The models used were: HadCM3L, the sister model of the FAMOUS model which is used in this study, [4]; ECHAM5/MPI-OM [43]; the GISS model [44] and two versions of the model CCSM. CCSM_H [3,45] which has no aerosol load following the approach of Andreae (2007) and Kump & Pollard (2008) [41,42] and CCSM_W [6,46] which has a modern aerosol load. At a given CO_2 concentration CCSM_H and CCSM_W give different global means. For instance, there is a 3 °C difference in Mean Annual Temperature (MAT) between CCSM_H and CCSM_W at 16x pre-industrial CO_2 concentrations, the level at which the best match to Eocene proxy data was found for that model. The range of CO_2 concentrations resulting in the best Eocene simulation between the models varied between 2x and 16x pre-industrial concentrations, demonstrating the need for better constraints on actual CO_2 concentration during the early Eocene.

A comprehensive comparison of model results with recent syntheses of proxy data was made [3,4] as part of the EoMIP, and a 1D energy balance model [43] was used to investigate, identify and understand the inter-model variability. The ACEX data points from the Arctic Ocean [7] indicate SSTs of ~13 °C for the Ypresian (56.0-47.8 Ma) and a SST of ~22 °C recorded during the Early Eocene Climatic Optimum (EECO, 53.1-49 Ma). Few of the models manage to simulate these temperatures. In the Southern Hemisphere, SSTs greater than 25°C are measured from both EECO and Ypresian material from ODP 1172D in the Pacific Ocean [11] and Waipara River of the coast from New Zealand [47]. Again only one model (CCSM_H) managed to intersect the lower error bars of these temperature estimates.

In summary, there is considerable inter-model variability between the models in the EoMIP. The variability is considerable larger than present day inter-model differences, with very different CO_2 giving the best fit to data. The differences between models have been attributed to a combination of greenhouse effect and surface albedo feedbacks rather than differences in cloud feedbacks or heat transport [4]. Differences in the climates of CCSM_H and CCSM_W are related to differences in the assumed aerosol loads used. Despite the variation in boundary conditions between these five models, only CCSM_H manages to simulate temperatures within the lower boundaries of the estimates at the warmest high latitude locations (i.e. ACEX, ODP 1172D and Waipara River), thus demonstrating the need for alternative solutions to the equable climate problems.

2.2 Parametrisations and ensembles

The EoMIP study highlights the inter-model variability between the models studied. Climate models are constructed by discretizing and then solving equations which represent the basic laws that govern the behaviour of the atmosphere, ocean and land surface [48] and many approximations are required in order to solve the nonlinear system of partial differential equations. Note that the solution of a partial differential equation depends on a) the initial conditions, b) forcing boundary conditions (focus of the previous paleoclimate studies), and c) approximations in form of climate parameterizations (this study).

Parameter uncertainty stems from the fact that small scale processes in all components of the climate system cannot be resolved explicitly in the climate system. This is the case in cloud processes for example [49,50]. Parameterisation of sub-grid scale processes is a major source of uncertainty in climate prediction [51], and whilst in some parameterisations the processes, observational evidence or theoretical knowledge is well understood, where this information is scarce the values chosen for a parameterisation may simply be because they appear to work [50]. Future climate change studies have recently focused on quantifying the uncertainty arising from these parameters using Monte-Carlo type techniques. [52]. This type of work is referred to as perturbed physics ensembles (PPE) because suites of simulations are generated by perturbing climate-sensitive model parameters. The resulting spread in predictions is quantified, leading to model-dependant probabilistic estimates of the distribution of future climate, warming and climate sensitivity. In a few cases, the ensembles are very large (i.e. a thousand member ensemble)

[52,53] but in most cases the number of simulations is limited by the computational cost of complex climate models to a few tens or a hundred simulations as is the case in [49,54].

Ensembles with perturbed climate-sensitive model parameters have begun to be used in paleoclimate research, primarily for the late Quaternary and particularly on the issue of climate sensitivity and ENSO e.g. [55–59]. Ensembles with perturbed climate-sensitive model parameters have also been used to “tune” the climate model to proxy data for the LGM [60]. However, few studies have investigated older time periods apart from a small set of simulations for the Pliocene [61].

In practice there are several hundreds of parameters that are poorly constrained in climate models and it is impossible to vary all of them. Gregoire et al., (2011) [60] identified a total of ten parameters to be varied in FAMOUS, of which six parameters had been tuned in a previous study [62] and recognised as having a high impact on the climate of HadCM3 [49]. The study by Murphy et al., (2004) [49] identified key parameters that had a major impact on Charney climate sensitivity (the global average temperature increase associated with a doubling in CO_2 and including a specific set of feedbacks).

This paper investigates the effect of parametric uncertainty on the early Eocene equable climate problem using the model FAMOUS. The motivation of this study is to attempt to detect ensemble simulations which match the proxy data available for the early Eocene and to understand how processes in these simulations vary from rest of the ensemble. We deliberately do not limit the parameter set perturbations to only those sets which perform well for modern conditions because we wish to explore if any combination of parameters are able to simulate the early Eocene equable climates.

3 Methods

3.1 Model description

FAMOUS (Fast Met Office/UK Universities Simulator) is an atmosphere and ocean general circulation model (AOGCM) which is based on HadCM3 (Hadley Centre Model version 3) [63]. Whilst its parameterisations of physical and dynamical processes are almost identical to those of HadCM3, FAMOUS has a reduced resolution in both the atmosphere and ocean, and a longer time-step which reduces the computational resources required to run FAMOUS to 10% of that required by HadCM3 [64]. This favours the use of FAMOUS in experiments where large amounts of computational resources are required.

The atmosphere component of FAMOUS is based on the Hadley Centre atmosphere model (HadAM3) (see [65] for full details). The atmosphere resolution in FAMOUS is 7.5° longitude x 5° latitude grid, with 11 levels in the vertical. The ocean model in FAMOUS is the Hadley Centre ocean model (HadOM3) (see [63] for full details) which is a rigid lid model. The ocean resolution in both FAMOUS is 3.75° longitude x 2.5° latitude grid with 20 levels and a 12-hour time step (using a distorted momentum equation) which is the same resolution as the model HadOM3L, and is lower than the resolution of HadOM3 (1.25° longitude x 1.25° latitude grid). Since the resolution of the ocean model is greater than the atmosphere, FAMOUS uses a coastal tiling scheme which combines the properties of land and sea in coastal grid boxes. The ocean model can then use the more detailed coastline allowed by its higher resolution grid whilst conserving coupled quantities [64]. FAMOUS does not use flux adjustments. Land processes are modelled with the UK Meteorological Office's land surface scheme, MOSES 1 [66]. Smith et al., 2008 [64] give a detailed description of FAMOUS and highlight the major differences between FAMOUS and HadCM3. The version of FAMOUS used in this work is identical to that of Gregoire et al., (2010) [59] and slightly differs from Smith et al., (2008) [61] as described in Gregoire et al., (2010).

The resolution of FAMOUS is not as high as the models used to investigate future climate change; horizontal resolution of the order of 1° to 2° degrees is now commonly used in the ocean component of most climate models [67]. However, FAMOUS fills an important niche in the current generation of models sitting between the higher resolution AOGCMs and the lower resolution, highly parameterised Earth System Models of Intermediate Complexity (EMICs). The reduced resolution allows us to fully spin-up the ocean, with some of our simulations extending to 8000 years. This would be impossible with the higher resolution models but is essential since the time scale for ocean equilibration is measured in 1000's of years.

3.2 Present day simulation

In the original tuning of FAMOUS, Jones et al., (2005) [62] systematically tuned the model to reproduce both the equilibrium climate and climate sensitivity of HadCM3. Smith et al., (2008) then undertook manual tuning to reduce a cold bias in the northern high latitudes, which led to the removal of Iceland. Gregoire et al., (2011) conducted ensembles with perturbed climate-sensitive model parameters for the present day and Last Glacial Maximum (LGM) climates. Building on this work, we use the present day control parameter values in Gregoire et al.'s (2011) configuration as our control present day simulation.

The present day version of FAMOUS uses the following concentrations of greenhouse gases: CO_2 – 280 ppmv; CH_4 – 760 ppmv; N_2O 270 ppmv. The orography is derived from the US Navy 10-min resolution dataset, with some small additional smoothing at latitudes poleward of 60° (see [64] for full details). The ocean resolution of FAMOUS does not allow for flow between the Atlantic and the Mediterranean. Instead a simple mixing has been parameterised for this region in an area which extends from the surface to a depth of 1,300m. An artificial island is used at the North Pole to avoid the problem of converging meridians [64].

3.3 Early Eocene model configuration and uncertainties

3.3.1 Paleogeography and orography

Paleogeographic reconstruction is a critical boundary condition in paleoclimate modelling, and reconstructing continental interiors, dimensions of paleo-orography, paleo-shorelines of ancient lakes and the widths of epicontinental seaways is challenging as the geological evidence left by these features can be minimal [68–71]. Modelling experiments have been used to explore the impact on climate for some of these poorly constrained variables. For example, experiments have investigated the impact of the inclusion of a large lake in western North America [32]; the opening and closing of the Arctic seaways during the early Paleogene [44] and the impact of uncertain orography [72] [27,73–75] on Eocene climate. Results suggest that uncertain paleogeography tends to increase regional uncertainty in modelled climate, with some potential for climatic tele-connections and modification of global climate.

The early Eocene simulations presented here use a paleogeography created using similar methods to Markwick and Valdes, (2004) [71]. The paleogeography is similar to the HadCM3 early Eocene simulations conducted by Tindall et al., (2010) [76] but at the resolution of FAMOUS. There is no flow between the global oceans and the Arctic Ocean in these simulations although opening these gateways could impact climate [44] and FAMOUS does not explicitly represent lakes.

3.3.2 Greenhouse gases and orbit

Early Eocene atmospheric CO_2 concentration is an important boundary condition with a large uncertainty. Proxy measurements indicate that CO_2 in the early Eocene was higher than present and estimates range from as low as 300 ppmv to > 4400 ppmv [7,15,77–81]. Climate modelling studies of the early Eocene have used different CO_2 values which span the entire proxy range. For these early Eocene simulations, CO_2 was set at 560 ppmv (2 x pre-industrial concentrations). Whilst this is at the lower end of the range of predicted CO_2 values for the early Eocene, it has been used because early Eocene sensitivity simulations (unpublished) showed that the Eocene configuration of FAMOUS is relatively sensitive to CO_2. All other greenhouse gases (CH_4, N_2O) were set to pre-industrial values. Indirect evidence indicates that during the early Cenozoic methane concentrations of these other greenhouse gases could have been much higher due to the expansion of peat lands and the consequent increase in methanogenesis for instance [82–85]. However, in the absence of suitable proxy data to quantify this increase we use present day values.

Orbital changes have been calculated for the past 250 million years (My), [86] and studies have identified a strong eccentricity and precession signal from early Eocene sediments [84,85,86]. We attempt to simulate a very long multi-million year interval in which many orbital configurations would have occurred. Whilst the role of orbital forcing may be a driver for short term hyperthermal events [83,90] we are interested in simulating the overall warmth of this period and thus have used a modern orbital configuration. Modelling studies which have investigated the impact of orbital forcing on the early Eocene climate have improved the model-data fit if specific orbits are chosen. Sloan and Morrill, (1998) [34] showed that extreme orbital values from the calculated Pleistocene range could reduce temperatures in the Northern Hemisphere continental interiors compared to the orbital configuration for the present day. Sloan & Huber, 2001 [33] showed that between precessional end members for an Eocene greenhouse world widespread regional variation occurred, including: SST variation of to 5°C in the high northern latitudes; up to a twofold variation in upwelling strength in tropical regions; and changes in net surface moisture balance (precipitation – evaporation) of up to 3mm/day in the tropics. Uncertainty in orbital forcing has a limited impact on global mean climate values and a larger impact on regional and seasonal climate, in particular at high latitudes. In the studies referenced here, [33,34] uncertainty was more pronounced in high latitude terrestrial realms and in the low latitude marine realm.

3.3.3 Vegetation

There is very little data available for vegetation reconstruction of past climates and the data that does exist may not be fully representative of the diversity of the area it comes from. Numerous modelling studies have investigated the impact of vegetation on paleoclimate [89,91–93] and several studies have looked specifically at early Eocene modelled vegetation [72,94,95]. Whilst the impact on global climate has been noted to be small, changes to regional climate can be distinct [72,94,95].

Vegetation in model simulations can either remain static and unchanging through time or dynamic and responding to the changing climatic conditions. Both approaches have advantages and disadvantages, as reviewed in Peng, (2000) [96], for example, dynamic vegetation may increase precipitation and reduce temperature extremes [97]. The work presented here used a static and uniform vegetation configuration of shrub-like plants everywhere as we consider the effect of vegetation feedbacks to be secondary compared to the parameter perturbations. Future work will examine the impact of vegetation change.

3.4 Perturbed Parameter Ensemble

Table 1 gives a description of each parameter perturbed in this work. We perturb ten parameters within their upper and lower bounds. The uncertainty bounds were based on previous studies [49]. The uncertainty arises because of the large spatial and temporal variation of many of these processes.

We have run two sets of perturbed physics simulations. In the first set all ten groups of uncertain parameters are perturbed simultaneously and at ten equal intervals between the lower and upper boundaries of their uncertain range, we refer to these simulations as the multiple parameter perturbations (MPP). In order to facilitate the best use of computing time and the greatest coverage of different parameter sets a statistical method of Latin hypercube sampling (LHS) is used to define the parameter values for the MPP simulations [98]. Using LHS with ten parameters requires in the order of one hundred simulations to obtain a reasonable coverage of the parameter space [99]. We therefore generated one hundred unique parameter sets, maximizing the parameter space that is sampled for a finite number of simulations in a statistically robust way. Full details of the LHS methodology are available in Gregoire et al., (2010) [60] who originally ran present day simulations with the same MPP sets. The MPP simulations were initially set up to run for 6,000 years, though runs of particular interest were integrated for 10,000 years. This length of the runs is required in order to achieve full equilibrium in both the surface and deep ocean in the early Eocene climate.

In order to understand some of the causes of the changes in climate, we selected a simulation with a promising early Eocene climate based on the 6,000 year results (from herein referred to as E6000). The climate in E6000 exhibited global warmth (MAT >30 °C) and polar regions with MAT > 10 °C. We used the ten groups of perturbed parameter values in E6000 to set up a further set of simulations in order to investigate the response of the climate to changes in one parameter at a time. This second group of experiments was termed the single parameter perturbations (SPP). We ran fifteen SPP simulations in total from the original ten parameter groups by separating the parameters in CW (threshold value of cloud liquid water at which precipitation commences) into land and sea components; the four parameters in the OCN_DIFF_H group, horizontal ocean diffusivity, were also split into three separate experiments. Finally OCN_DIFF_V, vertical ocean diffusivity and ATM_DIFF, horizontal atmosphere diffusion parameter groups were sampled twice: once using the values in E6000 and then a second set of simulations were conducting reducing the values even further than in E6000. These simulations are run for up to 9,000 years. A summary of the different sets of simulations and criteria used to assess them is shown in Table 2. Although E6000 does not make it into the final Eocene simulations; the parameter values of E6000 are shown in Table 4 for reference.

3.5 Present day simulations with 2x preindustrial CO_2

Present day simulations and with 2 x pre-industrial CO_2 concentrations (560 ppmv) were used to calculate Charney climate sensitivity values for the same MPP (multiple parameter perturbation) sets that were used in the early Eocene simulations (E_MPP). The present day configuration is identical to that described in section 3.2 with the exception of CO_2 concentrations of 560 ppmv were used. These simulations were run for 200 years.

3.6 Model-data comparison

Model output is compared to published multi-proxy datasets which have undergone comprehensive selection and standardization. We use the terrestrial dataset first compiled in Huber and Calallero, (2011) [3] and also available in Lunt et al., (2012) [4]. Our marine dataset is also from Lunt et al., 2012. An outline of the proxy data and consideration of the uncertainty associated with this data is given below.

The terrestrial proxy data set compiled by Huber & Cabellero (2011) contains fifty early Eocene data of Ypresian (56.0-47.8 Ma) and Lower Lutetian age. The Lutetian occurred between 47.8-41.3 Ma, however Lu1, the first global section of the Lutetian, is dated at 47.47 Ma thus we take the age span of the terrestrial data to be between 56.0-47.47 Ma. PETM (Paleocene-Eocene-Thermal-Maximum) and other hyperthermal events were excluded in the compilation of the dataset by Huber and Caballero, (2011). One middle Eocene data point ~45 Ma from the Tropics is included in the absence of any tropical data from the early Eocene [100,101]. There is no data coverage at latitudes greater than 65°S and coverage is highest in the Northern Hemisphere particularly over North America.

In order to account properly for systematic bias and spatio-temporal sampling uncertainty, the authors have reconstructed Mean Annual Temperature (MAT) based on Leaf-Margin Analysis (LMA) where possible. CLAMP (physiognomic analysis of leaf fossils) is used for MAT reconstruction when LMA is not available. MATs are calculated using the Kowalski and Dilcher, (2003) [24] calibration when feasible as this offsets the well established cool biases that may have been incorporated in the original calibrations [3 and references within]. Error bars are included in the terrestrial dataset to encompass the uncertainty introduced from the age of the material; topographic uncertainty and from the calibration method. All palaeolatitudes are adjusted to 55 Mya plate configuration utilizing the GPLATES software (www.gplates.org) and the plate model of Muller et al., 2008 [102]. Palaeo-elevation uncertainty is quantified by calculating the standard deviation of present day topography at elevations greater than 1,500m, and then applying this to an Eocene data to calculate the uncertainty in temperature as a result of lapse rate (±2.4°C), based on the work by Hren et al., (2010) [103].

The marine dataset used in this work was compiled by Lunt et al., (2012) and includes data from thirteen locations. The age range of the data spans the ages of ~55.0-49.0 Ma. Data is grouped into three categories by Lunt et al., (2012) and includes a) data aged ~ 55 Ma which is termed Late Paleocene data but excluding the PETM in [4]; b) well constrained EECO (early Eocene climatic optimum) data from between 53.1-49 Ma and c) early Eocene data which is constrained to the Ypresian, but not thought to be representative of the EECO. This final data set is referred to as background Ypresian. Given the recent new boundaries of the Ypresian (56-47.8 Ma) (www.stratigraphy.org) the Late Paleocene data referred to in Lunt et al., 2012 now is categorised as the earliest Eocene, thus, we term this data set the earliest Eocene. Multiple data are available at several locations where either two proxy methods have been utilised or data of different ages is available and our final marine dataset contains 15 data points in total. Data is generally well constrained with the exception of the data from Seymour Island in the Antarctic Ocean [9] which is provisionally classed as background early Eocene, although this may potentially be Middle Eocene in age.

Climate data is included from a range of proxies; $\delta^{18}O$ (planktic foraminifera), $\delta^{18}O$ (benthic dwelling molluscs), Mg/Ca (planktic foraminifera), clumped isotopes` and Tex^{86}. The authors have calculated three temperatures for the $\delta^{18}O$ data [76,104,105] in order to capture the upper and lower bounds of temperature estimates. Similarly three assumed values of Mg/Ca_{sw} values (3, 4 and 5 mol mol-1) are used to calculate Mg/Ca temperatures. There are now several published calibrations available for Tex^{86} and the 'high', 'low' and 'inverse' calibrations are all used. In addition samples with a BIT index greater than 0.3 are excluded where possible as this is now accepted as good practice (see Kim et al., (2010) for further details). However Ypresian samples from Tanzania [15] and Hatchetigbee Bluff, coastal North America, [106] were included by Lunt et al., (2012) despite higher BIT indices (0.3-0.5), in order to include more early Eocene data points.

We have averaged proxy temperatures calculated with different methods at the same location but we have not averaged data of different ages. As a result our dataset contains fifteen points that we use to compare to model output. The temperature ranges of these data points are summarised in Table 3. Minimum and maximum temperature estimates from the multiple proxy methods and calibration errors are plotted in all our estimates. The terrestrial dataset spans the ages of 56.0-47.47 Ma, and no divisions are specified. The marine dataset spans a slightly narrower age range (55.0-49.0 Ma) which is encompassed by the Ypresian, but has been subdivided into three categories: earliest Eocene, EECO and background Ypresian. Non EECO data (i.e. earliest Eocene and Ypresian) is referred to as the background early Eocene as it does not include the peak EECO temperatures.

A wide range of proxy data, using different methods have been used in these data sets which introduces uncertainty from numerous sources. For example uncertainties are associated with reconstructing paleolocation and depositional environments [72]; age control and diagenesis and alteration [107]. The geochemical effects on biological material are another source of considerable uncertainty, for example, whilst the effects of temperature and seawater $\delta^{18}O$ on foraminiferal $\delta^{18}O$ have been recognised for a long time [108], the effect of seawater CO_2 chemistry on foraminiferal $\delta^{18}O$ were only recognised through culturing experiments in the late 1990's [109,110]. This led to the realisation that foraminifera $\delta^{18}O$ based temperature estimates may be too low for periods of the past where atmospheric CO_2 was high, such as the early Eocene [77,111–113]. Better constraints on early Eocene CO_2 will also help improve temperature estimates from foraminiferal $\delta^{18}O$, however, other 'unknown' or currently unquantified factors which effect foraminiferal $\delta^{18}O$ may not have been recognised yet.

Similarly Tex^{86} is a relatively new paleothermometer [114] and understanding the environmental signal recorded by Tex^{86} for the early Eocene is exacerbated by use of this proxy outside of its calibration conditions. High latitude areas from which very warm early Eocene temperatures have been recorded by Tex^{86} (for example the Arctic Ocean) would have undergone several months of darkness due to the boreal winter, the lack of these organisms in the modern high latitude oceans make the use of this proxy method in polar regions problematic [115]. Incubation experiments are required to calibrate the Tex^{86} paleothermometer for tropical SSTs as the present day ocean is simply not hot enough [116].

Proxy data is compared point by point with model output at grid box resolution and with zonal mean values. Where the same land surface type is not present in the model as in the proxy data the nearest matching land surface location is used along a band of longitude. Terrestrial data is compared with the surface air temperature at 1.5 m in the model over terrestrial surfaces whilst marine data is compared to the ocean temperature at a depth of 5m.

4 Results

4.1 Successful runs

Some combinations of model parameters generated by our sampling technique result in climates which are far from realistic, for either a modern climate or a paleoclimate [60]. Moreover, in the extreme conditions of the early Eocene, 82 out of 100 Multiple Parameter Perturbation (MPP) simulations fail to complete due to the model generating very extreme climates (e.g. tropical temperature in excess of 50°C) resulting in numerical instabilities in

465 the model. Eocene MPP simulations were required to run for in excess of 10,000 years and Eocene Single Parameter Perturbations (SPP) ran for up to 9,000 years. A summary of the initial number of simulations; the selection criteria; and the final number of simulations for each set of experiments conducted are given in Table 2. It should be noted that in all Eocene simulations, we needed to perform multi millennial runs in order to reach near equilibrium in both the surface and deep ocean. In some cases, initial results from the first 1,000 years of the Eocene MPP simulations gave significantly different results. For instance, some simulations showed an 8°C change of global mean surface air temperature (MAT) between the end of 1,000 years runtime and the end of 10,000 years. The latitudinal gradients were also impacted such that in some simulations the equator-to-pole temperature difference (EPTD) changed by more than 15°C from 1,000 to 10,000 years. Even between 4,000 and 10,000 years, the gradient changed in some simulations by up to 5° C. The changes seemed to be strongly linked with the effects of ocean overturning and the time scales are consistent with this. These results highlight the potential for mis-interpretation of the climatic effects of model changes (either parameter or boundary conditions) if the simulations are less than a few thousand years in duration and justify the use of a relatively fast but comprehensive model such as FAMOUS.

482 In order to verify the stability of the Eocene simulations that completed 10,000 year runs, the time series of the global mean top-of-atmosphere (toa) net energy balance and global surface air temperatures were plotted against each other [117]. In three simulations global surface air temperature appeared to be in equilibrium but the toa net energy was not tending to zero and so these simulations were discarded. In the remaining 17 Eocene simulations (15 MPP and 2 SPP) the global mean net toa energy balance is less than 0.3W^{-2} (and is most cases less than 0.1 Wm^{-2}) indicating that the simulations were in radiative balance. Trends in time series plots of global mean annual surface air temperature are small in the final simulation set with most simulations varying less than 2°C over the final 1000 years of simulation.

4.2 Climate of the final simulations

493 In initial condition ensembles, model parameters and forcings are identical throughout the ensemble but each simulation has a different starting state. In these ensembles the natural variability in the system is of interest and thus an ensemble mean value is a useful measure. In perturbed physics ensembles (PPE) such as the work described here, model parameters

and forcings have been changed whilst the initial conditions are identical. The value of PPEs is in understanding where and how the climate converges and diverges within the ensemble. We therefore describe the range of climates simulated but do not present the ensemble mean.

The parameter values of the final simulations and of the control parameter set are given in Table 5. The simulations are ranked in order of ascending global mean annual temperature (MAT) and this ranking is used to identify the different simulations, i.e. the simulation with the lowest MAT is termed E1 and simulation with the highest MAT is referred to E17. We performed simple regression analysis of each parameter against a number of global annual climate values (i.e. MAT, MAP, tropical SSTs, polar SSTs, equator to pole temperature difference planetary albedo, low cloud and high cloud global values) but the resulting R^2 correlation coefficients were all below 0.5 indicating that direct correlation between these variables are not strong and that it is the combination of changes which are key.

4.2.1 Temperature and precipitation

Table 4 summarises some climate variables for the final seventeen simulations. MAT in our "final" simulations range from 12°C to 32°C, mean annual precipitation (MAP) ranges from 2.7 to 4.1 mm/day and there is a strong positive correlation between MAT and MAP, with an R^2 of 0.97 and a slope equivalent to a 0.76 mm/day (~25%) increase per 10°C. This strong relationship also holds for the land and ocean precipitation i.e. the fraction that falls over land versus ocean (~30% of total precipitation falls over land) remains approximately constant across the range of simulations.

Figure 1 shows the MAT averaged from years 9,900-10,000 for two example runs; simulation E1 which has the coldest global mean temperature of 12.3 ˚C and the warmest model, E17, with a much higher global mean temperature of 31.8 ˚C. Not surprisingly, the basic spatial patterns are quite similar between the two simulations but with a large offset of ~ 15 °C. In E1 (Fig. 1a), the mean annual temperatures are significantly below zero at high latitudes in both the North and South. These cold temperatures are even more pronounced seasonally (not shown) as temperatures decrease below -20 °C in large parts of the high latitude continents. By contrast, annual mean temperatures in the warmest models remain above freezing for almost the whole globe. Simulations E16 and E17 have no annual mean temperatures below zero and E15 has a small area of sub-freezing temperatures (reaching -10 °C) in the very heart of Antarctica, although the coastal regions of Antarctica remains above freezing. Seasonally, there are still some sub-freezing temperatures but in the warmest models, these are confined to very small regions in the heart of the continents polewards of about 60°N and S and in regions where there are no proxy data to evaluate such values.

The spatial patterns of precipitation for simulation E1 and E17 are shown in Figure 2 for both summer and winter seasons. The patterns over land are broadly consistent between warm and cold models but with some of the most marked differences in precipitation occurring at high latitudes. In E1, the North Pole is a "polar desert" (shown clearly in Figure 2a), whereas in E17 the poles are relatively moist. This is unsurprising given the much warmer and sea-ice free polar regions in the warm model. In the tropics, there are some important differences particularly over the ocean where the cold model shows a distinct split ITCZ (also clear in Figure 2a) whereas the warmer model has a much broader feature and centred on the equator. However, over land there are somewhat smaller differences in the patterns of precipitation. In both simulations, the sub-tropics are seasonally dry but annual averages reveal only very small areas which are dry throughout the year.

4.2.2 Equator to pole temperature difference

Although some simulations achieve very warm polar temperatures, they also have very warm tropical temperatures so that the resulting equator-pole temperature gradients (EPTD) are generally very similar to present. EPTD are calculated for all simulations by subtracting mean polar temperatures (70°N to 90°N and 70°S to 90°S) from the mean equatorial temperatures (10°N to 10°S). We have calculated the marine EPTD for the present day control simulation (Table 5), and the Northern Hemisphere (NH) marine EPTD is 27.2 °C. Marine EPTD in the coldest and warmest Eocene simulations E1 and E17 are both 25.1 °C. Intermediate models (E7 to E15) have a greater NH marine EPTD of up to 31.9°C. In these intermediate simulations sea ice acts as a buffer, keeping the marine temperatures at high latitudes around 0 °C. Once this reduces, polar oceans begin to warm which then reduces the gradient. Examination of the equivalent terrestrial gradients helps confirm this as it shows a simpler gradual reduction in temperature gradient between the coldest and warmest models. The NH terrestrial EPTD for the present day is 39.2°C. The NH terrestrial EPTD for simulations E1 to E15 range between 38.2°C and 43.5°C, whereas E16 and E17 have a NH terrestrial EPTD of ~32°C, a 6-7°C reduction compared to the present day. The Southern Hemisphere (SH) terrestrial EPTD for the present day is very large (58.4°C) due to the ice covered Antarctic. During the early Eocene, with no ice and no circumpolar current, the largest SH terrestrial EPTD for the Eocene is 42.7°C. However, the warmest Eocene models have a terrestrial equator to pole gradient of ~30.5°C which is a notable reduction. The SH marine EPTD in the present day simulation is 27.8°C, and the majority of the Eocene simulations have a SH marine EPTD between 24.6°C and 28.9°C. Three simulations have a smaller SH marine EPTD, these are E14 (20.9°C); E16 (22.9°C) and E17 (20.1°C). Thus, in our two warmest Eocene simulations (E16 and E17) terrestrial EPTD in both hemispheres and SH marine EPTD do show a small reduction in temperature gradients in both hemisphere, which is compatible with the reduced EPTD suggested by the sparse data available for the Eocene.

The 6x pre-industrial CO_2 HadCM3L simulation in the EoMIP [115] had the least polar amplification of temperature from the five models compared. HadCM3L is an intermediate model (resolution) between HadCM3 and FAMOUS. As it is part of the same family of models as FAMOUS we compare the EPTD as calculated using the method above with these simulations. In the Northern Hemisphere SST EPTD is 29.7 °C and the Southern Hemisphere SST EPTD is 26.3 °C. These EPTD are larger than those in our present day control but are well within the EPTD range simulated by the Eocene ensemble, maximum values of which are 32.2 °C for the NH and 29.0 °C for the SH.

4.2.3 Other Climate Characteristics

The sensitivity of the early Eocene, proto-Atlantic ocean meridional overturning circulation to changes in the concentration of CO_2 (which changed the warmth and the presence of sea ice) was described in Lunt et al., (2012) for HadCM3L. We find similar results for the Atlantic overturning circulation in our suite of simulations. The warmer the simulation, the stronger the Atlantic intermediate-water formation, with a jump in the strength between simulations E6 and E7 related to a loss of year round sea ice in the North Atlantic. Further increase in Atlantic-intermediate-water formation in the very warm simulations (E14-E17) is associated with the almost complete loss of seasonal sea ice. However, the location of oceanic convection, as indicated by the mixed layer depth, remains quite similar in all models. An intermediate to deep anticlockwise flow develops in the models where sea ice disappears in the South Pacific (e.g. simulations E9, E14, E16 & E17). The centre of the cell is between 1000 m and 2000 m with the bottom of the cell extending to 4000 m in E16 and up to 3000 m in E9, E14, E16 and E17. This replaces a deeper, small bottom water cell in the cooler models which have year round South Pacific sea ice. In addition to the high latitude sources, there is also a source of intermediate water within the Tethys seaway. The relatively enclosed basin is very warm and experiences high evaporation. As a consequence, the surface waters are sufficiently saline to sink and these then spread out at about 2km depth (Figure 3).

A substantial increase in tropospheric mid-latitude westerlies which increase by more than 25% between coldest and warmest simulation is observed. Moreover the strength of the tropical easterlies weaken considerably but do not transition to westerlies as seem in [116]. It is likely that some of this difference is related to the resolution of FAMOUS which does not represent the atmospheric wave dynamics (particularly the Madden Julian Oscillation) reported in [119]. The strengthening of the westerlies in our simulations seems to be strongly linked to a much intensified Hadley cell.

4.3 Model-data comparison

Figure 4 and Figure 5 show respectively the zonal means for the mean annual SSTs and terrestrial MATs for all seventeen final simulations. The marine and terrestrial proxy datasets [3,4] are overlaid in these plots along with the lower and upper temperature bounds and the calibration errors for each data point. No simulation has a MAT or SST zonal mean that intersects all the proxy points (including the error bars).

In order to assess rigorously how well each simulation matches the proxy temperature estimates we calculate the root mean square error (RMSE) for the difference between the simulation temperature predictions and the proxy data temperature estimates for all marine and terrestrial data (see Table 6). RMSEs for the different time periods included in the marine dataset have also been calculated (i.e. Ypresian, earliest Eocene and EECO) as have RMSEs for mid and high latitudes in the terrestrial data set. Low RMSE values indicate that there is a better model-data fit than large RMSEs. Simulations E1 to E10 have greater terrestrial RMSEs than marine RMSEs, whereas simulations E12 to E17 have greater marine RMSEs than terrestrial RMSEs indicating that above 22.1°C (MAT of E11) an improved fit with terrestrial proxy data is at the expense of the fit with the marine dataset.

Differences between the proxy temperature and simulation temperature estimates have been calculated for the marine and terrestrial datasets and are shown in Figure 6 and 7. These are used to assess how well the simulations match the proxy data and to visualise any bias in the simulations. The simulation errors in the terrestrial data (Figure 6) have an 'approximately' normal distribution. Simulations E1 to E15 consistently under predict terrestrial temperatures (e.g. the distribution is centred below zero). Simulations E16 and E17 over and under predict an equal number of terrestrial data points by up to +/-10°C (e.g. the distribution is centred about zero). Figure 7 shows the differences for the marine dataset. There are not enough marine data points to assess the distribution of the data. Many of the simulations are skewed to the right indicating an over prediction of SSTs. Simulations E14 and E15 are centred near zero and over predict SSTs in half the data points by up to 5°C but under predict the remaining SSTs by between 10°C and 20°C. Simulations E16 and E17 are also centred near to zero, both simulations over predict SSTs in half the data set by up to 10°C and under predict SSTs by the same amount (E17) or slightly more, up 15°C (E16).

The four warmest simulations (E14 to E17) all consistently over predict SSTs at four locations. These are the Ypresian age data recorded at Tanzania and Hatchetigbee Bluff and the Earliest Eocene data from ODP 865 and ODP 1209 and Seymour Island. E14 has the smallest error and E17 has the largest error in all these locations, with the error varying between 1 °C to 11 °C at these locations. Three of these locations have specific uncertainties associated with them, uncommon with the other marine data points. The data at Tanzania and Hatchetigbee Bluff were included in the marine data compilation despite having BIT indexes between 0.3 and 0.5, indicating a large terrestrial organic matter component in the data signal. This has increased uncertainty in the SST estimate [120,121] but to what degree is not stated. Similarly the data from Seymour Island has provisionally been aged as earliest Eocene, however, the possibility of this data being Middle Eocene age has been raised [122]. If this data is re-assigned to a Middle Eocene age it may be assumed that early Eocene temperatures at this location would be higher. The over estimate at Seymour Island is the greatest for simulations E14-E17 from the marine dataset and this is possibly the marine data point with the largest age uncertainty. Better age constraints at Seymour Island will allow this uncertainty to be resolved in the future. In contrast the Middle Eocene age tropical data point included in the terrestrial data set actually compared reasonably well with the warmest simulations: temperatures are ~1.2 °C and 2.9°C warmer than the proxy temperatures in simulations E16 and E17, which are well within the published error bars for this data point.

Three marine locations are consistently too cold in the Eocene simulations, all of which are high latitude EECO aged data points. The data are from the ACEX core in the Arctic Ocean at a latitude of ~83°N [7]; Waipara river off New Zealand at a latitude of ~54°S [47,123] and at ODP 1172D in the south west Pacific at a latitude of ~64°S [11]. The paleo-reconstruction of all three of these locations is for a shallow marine environment, with Waipara river and ODP 1172D being coastal and from restricted environments. The ACEX data point, although in a restricted basin, is in the most open setting. There are two factors that may contribute to the under estimation of temperatures at these locations, these are the bathymetry in the model and the use of a static orbital configuration. The original references (see Table 3) for these proxy data identify these locations as shallow water or restricted environments with water depths of up to ~ 2,000 m, however, the bathymetric reconstruction in our model is a between 2,000 m and 3,000 m at all these locations. There is evidence of orbital forcing pacing the EECO climate [87–89]. Previous modelling studies which have investigated orbital forcing during the early Eocene identified the climate of the high latitude terrestrial realm as being sensitive [33,34]. Further work with a dynamic orbital configuration may reduce the model-data discrepancy with the EECO proxy data

Overall, differences between the terrestrial data set and the simulations are much smaller than with the marine data set, particularly in simulations E16 and E17. Temperatures at three locations in North America are consistently over-predicted by ~10°C by simulations E16 and E17 compared to proxy temperatures. These locations are all along the south or west coast of North America which was mountainous during the early Eocene. The uncertainty in orographic reconstruction in these particular locations are high and close to ± 1,000 m [3]. Huber & Cabellero, (2011) calculate the temperature uncertainty associated with orographic uncertainty in the terrestrial data set as ± 2.4 °C for an uncertainty of ± 450 m based on the environmental lapse rate of 5.2 °C/km [103]. Given the larger orographic uncertainty at these locations and the coarser resolution of the land surface in our model than CCSM_H, the model this data set was prepared for comparison with, a larger temperature error of at least ± 5.2 °C may be more representative here, and which provides a much improved fit between simulations and proxy data.

Taking the marine and terrestrial comparisons together, of the seventeen final simulations, two simulations have a more optimal fit with the early Eocene proxy data; these simulations are E16 and E17 which are the simulations with the highest MAT. The MAT of the best performing simulations for each model in the EoMIP study range between 24.0 °C and 29.5°C, with the ECHAM model (2x CO_2) and HadCM3L (6x CO_2) at the bottom end of this range and CCSM_H (16x CO_2) at the upper end. Our two best simulations both have higher MATs than the EoMIP models. The two optimal Eocene simulations are described below:

- E16 (MAT of 29.7 °C) is a single parameter perturbation where the horizontal atmospheric diffusion parameter (atm-diff) was reduced to 72 % of control value, the parameter choice in this simulation was based on the parameter values in a promising Eocene multiple parameter perturbation simulation at ~4,000 years (the original simulation this was based on did not make it into the final selection)
- E17 (MAT of 31.8 °C) is a multi-parameter perturbation where all ten uncertain parameters were varied together in order to maximise the parameter space sampled in these experiments

These two simulations also have marine and terrestrial EPTD which are at the lowest end of the simulations. These simulations are much better at reproducing high latitude Southern Hemisphere warmth than Northern Hemisphere warmth. Whilst neither simulation manages to replicate the high temperatures recorded in the marine EECO proxy data, the global warmth of the early Eocene is captured. E16 & E17 do have limitations and neither fit the proxy data perfectly, however, investigating how climate processes and heat transport differ in these simulations, may give us insights into understanding low polar seasonality and continental warmth during the Eocene.

4.4 Are the models too hot?

It should perhaps also be noted that the tropical SSTs in the warmest models are very warm. The zonal mean SST is almost 40°C and in places within the tropics it even exceeds 42°C. Such high temperatures exceed the optimum for many modern day species of ocean biological processes [124,125] such as growth. Thresholds in foraminifera with symbiotic algae have also been linked to enzyme inactivation at temperatures >35°C [124]. However, it should be noted that these temperatures decrease away from the equator so that by about 15°N and 15°S they are nearer 35 °C. Similarly, at a depth of 50 m the temperatures have decreased to 36 °C. Temperature is a strong biogeographic control on ocean biota and reduced zonation of foraminifera and poleward migration of foraminifera have been shown during the early Cenozoic [126,127]. Similarly the selective extinction of warm water ocean taxa during subsequent climatic cooling events such as at the Eocene-Oligocene transition [127] indicate that modern foraminifera are not representative of greenhouse climates such as the Eocene and the possibility that species can adapt to the extreme conditions these temperatures indicate cannot be ruled out [128]. Conversely, for the EECO marine data points, the data may not be hot enough. The uncertainty associated with biological proxy data from past warm periods where continues to be problematic and the omission of strong orbital forcing in our model may preclude these temperatures from being simulated in this ensemble.

4.5 Causes of the warmth

While it is relatively easy to analyse the reasons for the warmth in these simulations relative to the present day control climate it is more difficult to analyse the causes of the warmth between the two warmest models. If we compare simulations E16 & E17 to the present day control simulation we see that there are a number of drivers of change beyond the increase in CO_2. Firstly, the relative humidity within the simulations remains relatively constant (albeit with some small decreases at high latitudes in the mid-troposphere) so that the specific humidity increases at all levels and latitudes in the warmer simulations (E16 and E17) compared to the colder simulations (E1 – E15) and the present day simulation (PI), resulting in a strong positive feedback from water vapour.

Secondly, the removal of land ice greatly decreases the surface albedo. However, this is not a straightforward feedback. In the colder runs, the land ice is largely replaced by heavy snowfall so that the global mean surface albedo does not change appreciably (Table 5). However, in the warmer climate simulations there is a major decrease in snow cover and hence we have a strong positive feedback. Sea ice also experiences major decreases in the warmest simulations.

The planetary albedo follows a similar relationship as surface albedo, with decreased albedo with warmer temperatures. As MAT increases in the ensemble, there is also an increase in net solar radiation at the top of the atmosphere (toa) indicating increased radiative forcing. However, there are some more complicated variations from this simple pattern. Specifically simulations E12 and E15 increase their planetary albedo compared to the overall downward trend and subsequently reduce the net solar radiation toa relative to the remaining simulations. This appears to be strongly linked to changes in cloud cover.

Overall, the warmer models generally have less total cloud cover which is consistent with the idea that clouds are acting as a positive feedback in these simulations. Moreover, the total cloud cover is strongly correlated with the planetary albedo (Table 5). However, the patterns are quite complicated. Low clouds have a tendency to cool the climate system (through their impact on albedo) and hence the large reductions in this type of cloud in our simulations are producing a positive feedback. However, high clouds also decrease which moderates this somewhat. At higher latitudes, all types of clouds act to warm the climate system and in most of the simulations we have an increase in high latitude cloudiness. The ratio of low clouds to high clouds decreases as MAT throughout the ensemble, in E1 this ratio is 1.1 and in E16 and E17 this ratio is 0.8 and 0.9 respectively. Further complicating matters, the parameters perturbed in these simulations impact cloud physical properties such as cloud water content, cloud ice content and subsequently cloud albedo. These variables were not output in these simulations and would need to be assessed alongside any changes in cloud amounts before any definitive conclusions on the radiative balance can be drawn, particularly in relation to the processes suggested in previous studies such as polar stratospheric clouds [28,37,38,129] and high latitude convective cloud feedbacks [39,40130130,131]

In terms of changes in EPTD (Equator to pole temperature difference), it is also useful to examine the poleward heat transport in the simulations. Peak values of heat transport (HT) occur at ~40° latitude in the Eocene ensemble and in the present day control. In the present day simulation peak values of HT are 5.3 PW in the Northern Hemisphere (NH) and 4.9 PW in the Southern Hemisphere (SH). In the Eocene ensemble, peak HT ranges between 5.1–6.0 PW in the NH and 5.0-5.7 PW in the SH. At the latitude of peak HT, atmospheric heat transport (AHT) accounts for between 89-94% of heat transport in the Northern Hemisphere and 85-93% of heat transport in the Southern Hemisphere. For the modern, peak values of HT are ~5 PW at 35° latitude, with AHT comprising 78% and 92% of the total heat transport in the northern and Southern Hemispheres in good agreement with [132]. Ocean heat transport (OHT) peaks much closer to the equator and can be important at those latitudes but is relatively unimportant further polewards. Figure 8 shows the distribution of HT for the present day and for the warmest Eocene simulations. The range of OHT in the Southern Hemisphere and of AHT in the Northern Hemisphere are particularly large but the total variation is always dominated by the atmosphere.

The OHT acts to transfer heat from the tropics to higher latitudes and to weaken the latitudinal temperature gradient. The correlation between tropical ocean temperatures and OHT is clearly shown in figure 9a. However, the link between OHT and equator to pole temperature gradient is less clear (figure 9b) This is because of two reasons. Firstly the ocean heat transport is not strong, and is almost negligible beyond about 45° N and S, and hence has its strongest effect on mid-latitudes. Most of the heat transport further polewards is performed by the atmosphere. Secondly, the link between total heat transport and equator to pole temperature gradient is also complicated because the albedo varies between the simulations. This implies that the total heat transport required to maintain the gradient will also vary [133].

4.6 Equivalent modern simulations

Of the fifteen MPP simulations in the final seventeen Eocene simulations, only one parameter set (from E17) surpasses the control parameter set for a present day simulation in the present day (see Table 2 for criteria used to assess present day simulations). The present day equivalent of the Eocene MPP simulation E11 is ranked only one place behind the control simulation in the present day ensemble. The control parameter set, however, does not make it into the final ensemble of Eocene simulations.

For all of the fifteen final Eocene MPP simulations, we have an equivalent present day control and 2x CO_2 concentration simulation. Thus it is possible to calculate the Charney climate sensitivity for these parameter sets. The Charney climate sensitivity is broadly defined as the equilibrium global mean surface temperature change following a doubling of CO_2 concentration. The mean ±1 standard deviation values for Charney sensitivity for the eighteen models assessed in the Fourth Assessment Report (AR4) of the IPCC [134] was 3.26 °C ± 0.69°C. Of the subset of our fifteen simulations which are run at 2xCO_2 concentration the mean ±1 standard deviation values for the Charney sensitivity is 3.25 °C ± 0.58 °C, which is very similar to the AR4 mean value. The Charney sensitivity for our bets model, E17, is calculated to be 2.7 °C, which is below this mean estimate. CCSM3, which was used for the Eocene simulations by [3,45] has a present day climate sensitivity of 2.7 °C, whilst HadCM3 the sister model of FAMOUS has a Charney sensitivity of 3.3 °C. Thus, our best performing parameter set for the Eocene, and which was able to simulate the extreme warmth of the Eocene, actually has a reduced climate sensitivity compared to the control parameter set, and a very similar climate sensitivity to CCSM.

Moreover, Gregoire et al., (2010) use the same 100 MPP parameter sets in their tuning study which focused on the present day and the last glacial maximum (LGM). Simulation S4 which is highlighted in their study as having a favourable fit has identical parameters to our Eocene simulation E17.

5 Conclusions

Our work is the first attempt at a comprehensive ensemble with perturbed climate-sensitive model parameters for the early Eocene. The results show that we can get a large diversity in response, with global mean temperature changes which vary considerably, from temperatures which are slightly cooler than the modern, to temperatures which are extremely warm. We have managed to simulate levels of warmth comparable to that of the early Eocene at only 2x pre-industrial CO_2 which is a much lower concentration than used by many other models.

Although many aspects contribute to this warmth, a strong sensitivity to albedo changes associated with cloud cover was apparent. Clouds remain one of the most uncertain aspects of climate modelling with little consensus over the sign of the cloud feedback. In this work the choice of perturbed parameters affected the physical properties of the clouds. The physical properties of the clouds and the effect on radiative balance will be examined in future work.

Within the ensemble, as mean annual temperature (MAT) increases ocean heat transport decreases in both the Northern and Southern Hemispheres. In the Southern Hemisphere as tropical SSTs increase and polar SSTs increase this also correlates to a reduction in ocean heat transport. However, this relationship is not apparent when ocean heat transport and the equator to pole temperature difference (EPTD) are compared across the ensemble. This implies that ocean heat transport is not a major control on the EPTD. If ocean heat transport is not a major part of the EPTD, atmospheric heat transport and local radiative effects are the likely to be involved in driving changes in the EPTD.

Proxy-model discrepancies are larger in the marine dataset than the terrestrial data set. Simulation of the marine early Eocene climatic optimum (EECO) temperatures are the most problematic, with the warmest simulation still 12 °C too cool compared to the proxy Tex^{86} temperature estimated. Some of this temperature difference may be attributable to the use of a modern orbital forcing in these simulations. There is evidence for a strong precessional and eccentricity signal pacing the EECO, all the EECO data used in this study are from the high latitudes and previous studies indicate that the high latitudes are most sensitive to orbital forcing during the Eocene [33,34] and other periods [135,136].

It has been known for some time that perturbing the parameters of models can result in a wide spread of results. However, one of the most exciting aspects of our results is that the "best" climate simulation for the early Eocene was also one of the best simulations for the present day and Last Glacial Maximum. For the Early Eocene, our results have to be partly tempered by the uncertainty in boundary conditions, particularly the lack of a precise indicator of past greenhouse gas concentrations. Therefore we may be obtaining a good comparison to data for the wrong reasons.

When we apply this parameter set to a future climate change simulation, we find that the resulting temperature increase due to an instantaneous doubling of CO_2 (so called Charney climate sensitivity) is 2.7°C. This value is slightly below the mean estimates of Charney sensitivity from the IPCC Fourth Assessment Report [134]. This is perhaps surprising since there have been indications [137] that paleoclimate data would imply that models were under sensitive. Our new results show that it is possible that a model can respond strongly to past changes without it necessarily resulting in a high sensitivity to future changes.

Paleoclimate research focused on comparing proxy data to models will never be able to "prove" that climate models work. However, it does provide a unique test of models ability to simulate climates different to present. It is worth bearing in mind that even with an optimal choice of parameters there will be irreducible structural deficiencies in the model that cannot be mitigated. However, it is still very encouraging that a single model parameter set exists which results in a model that simulates well the present day, Last Glacial Maximum, and early Eocene.

6 Acknowledgements

The authors would like to thank the two anonymous reviewers for particularly helpful suggestions and comments. This work was carried out using the computational facilities of the Advanced Computing Research Centre, University of Bristol,

http://www.bris.ac.uk/acrc . The Eocene paleogeography was created by Fugro-Roberstson.

The simulations described in this work are available at the following website http://www.bridge.bris.ac.uk/resources/simulations

No.	Parameter name	Parameter description	Max	Int.	Min
1	**RHCRIT**	Threshold of relative humidity for cloud formation	0.9	**0.687**	0.6
2	**VF1**	Precipitating ice fall-out speed	2	**1.75**	0.5
3	**CT**	Conversion rate of cloud liquid water droplets to precipitation	4.00E-04	**9.41E-05**	5.00E-05
4	**CW***	Threshold value of cloud liquid water for formation of precipitation over the sea and over land			
	CW_SEA		5.00E-04	**3.82E-05**	2.00E-05
	CW_LAND		2.00E-03	**1.61E-04**	1.00E-04
5	**G_WAVE**	Gravity wave parameters (2 parameters)			
	K_GWAVE		2.00E+04	1.50E+04	**1.00E+04**
	KAY_LEE_GWAVE		3.00E+05	2.20E+05	**1.50E+05**
6	**Z0FSEA**	The free convective roughness length over the sea for boundary layer processes	0.005	**0.00111**	0.0002
7	**ALPHAM**	Albedo (reflectivity) of sea ice variability with temperature	**0.65**	0.5	0.2
8	**ATM_DIFF**	The horizontal atmospheric diffusion parameters varied together (2 parameters)			
	DIFF_COEFF		4.19E+09	3.85E+09	**3.50E+09**
	DIFF_COEFF_Q		2.40E+08	2.20E+08	**2.00E+08**
9	**OCN _DIFF_H****	Oceanic horizontal diffusion parameters varied together (4 parameters)			
	FNUB_SI		1.10E-05	**1.00E-05**	8.00E-06
	KAPPA0_SI		1.10E-05	**1.00E-05**	8.00E-06
	DKAPPA_DZ_SI		3.08E-08	**2.80E-08**	2.20E-08
	FNU0_SI		0.00605	**0.0055**	0.005
10	**OCN _DIFF_V**	Oceanic vertical diffusion parameters varied together (6 parameters)			
	AM0_SI		1.65E+05	**1.50E+05**	1.20E+05
	AM1_SI		1.65E+05	**1.50E+05**	1.20E+05
	AHI1_SI		1100	**1000**	800
	AHI2_SI		1100	**1000**	800
	ATHKDF1_SI		1100	**1000**	800
	ATHKDF2_SI		1100	**1000**	800

Table 1 – Name and description of the ten parameters or groups of parameters that are perturbed in this study. The minimum, maximum and intermediate values for each parameter are also given with the standard value highlighted in bold. The parameters are derived from the uncertainty study by (Murphy et al. 2004) and from known climate sensitive parameters in FAMOUS as described in (Gregoire et al. 2011). RHCRIT, VF1, CT, CW_LAND and CW_SEA are all involved in cloud processes. ATM_DIFF, OCN_DIFF_H and OCN_DIFF_V are associated with diffusion processes. The elements of CW are varied as a pair in the MPP (multiple parameter perturbations) but are perturbed separately in the SPP (Single parameter perturbations).

ID	Description	Details	Assessing the simulations	Final
PD_MPP	100 pre industrial MPP (multiple perturbed parameter) ensemble run initially for 200 years, with a subset continued for an additional 300 years (500 years in total)	10 parameters perturbed as identified from (Murphy et al.,2004) and from climate sensitive parameters in the model FAMOUS (Gregoire et al., 2011). Perturbed parameter sets were generated using Latin hypercube sampling (LHS) (See Gregoire et al., 2011 for full details)	An Arcsine Mielke [Watterson 1996] score was calculated for all 100 simulations and the control simulation (see Gregoire et al., 2011). Simulations with a higher Arcsin Mielke score than the control (14) and the control simulation were continued for an additional 300 years. Thus 86 simulations were not continued.	14 simulations and control simulation with standard parameter set were run for 500 years.
E_MPP	100 Eocene MPP (multiple perturbed parameters) ensemble run for up to 10,000 years	Parameter sets are identical to those in PI_MPP	Successful simulations ran for the allotted time (10,000 years) and had stable toa (top of atmosphere) net energy balance and surface air temperatures. 59 simulations failed within 100 years; a further 4 failed to complete 1000 years, and 19 failed to complete 4,000 years. 18 simulations complete 10,000 years of which 3 are identified as unstable. Simulation E6000 is one of the 3 unstable simulations.	15 simulations run for up to 10,000 years. Three parameter sets overlap with the final PI_MPP simulations
E_SPP	14 Eocene SPP (single perturbed parameter) ensemble run for up to 9,000 years	Based on the climatologies of E_MPP at 6000 years, a simulation with a promising Eocene climate (E6000) was selected and used as the basis of the SPP. 8 parameter sets were varied as in E6000; Parameters in CW and OCN_DIFF_H were varied separately to create 5 further simulations. DIFF_COEF and DIFF_V were reduced further than in E6000 to give an additional plit to give 2 further simulations; and DIFF_COEFF and DIFF_V were reduced further than in E600 to create 2 further simulations.	Simulations were deemed successful if they ran to their allotted time and were stable as assessed by top of energy net energy balance and surface air temperature drift. Only 3 simulations completed their time, of which one was unstable.	2 simulations run for up to 9,000 years

Table 2 – Summary of the three groups of experiments discussed in this paper and the criteria used to assess and rank these simulations. The three groups of experiments are: PD_MPP, A present day 100 member multiple perturbed parameter ensemble; E_MPP, an Eocene 100 member multiple perturbed parameter ensemble and E_SPP, an Eocene 14 ensemble single perturbed parameter ensemble. In the PI_MPP only 14 simulations outperform the control parameter set. Only 15 E_MPP and 2 E_SPP simulations are deemed successful, which does not include the control parameter set.

LOC_ID	ID	Paleolatitude	Paleolongitude	Median MAT (°C)	Maximum MAT (°C)	Minimum MAT (°C)	Calibration (+/-°C)	Proxy method	Age	SITE_ID	Original references
1	1	-65.3	-1.2	13.2	16.9	7.2	0.7	Foram. $\delta^{18}O$	Background Ypresian	ODP 690	Stott et al. (1990)
2	2	-65.7	-59.5	11.7	18.4	2.0	1.4	Mollusc $\delta^{18}O$	Background Ypresian	Seymour Island	Ivany et al. (2008)
3	3	-61.1	79.3	13.8	17.1	10.3	0.7	Foram. $\delta^{18}O$	Background Ypresian	ODP 738	Barrera and Huber, (1991), Lu and Keller, (1993)
4	4	-63.9	156.8	24.9	28.9	23.1	4.0	Tex_{86}	Background Ypresian	ODP 1172D	Bijl et al. (2009)
4	5	-63.9	156.8	29.0	30.0	24.5	4.0	Tex_{86}	EECO	ODP 1172D	Bijl et al. (2009)
5	6	-54.2	-163.7	27.4	29.0	25.4	2.5	Tex_{86} and Mg/Ca	EECO	Waipara River, NZ	Hollis et al. (2009) and Creech. (2010)
6	7	-18.0	34.6	30.7	32.1	27.3	2.3	$Tex_{86\ and\ d18O}$	Background Ypresian	Tanzania (TDP14, 7, 3)	Pearson et al. (2007)
7	8	30.8	-71.6	27.7	29.4	25.2	3.0	Clumped isotopes and Tex_{86}	Background Ypresian	Hatchetigbee Bluff, Al	Keating-Bitonti et al. (2011)
8	9	83.2	28.9	22.4	14.5	11.1	4.0	Tex_{86}	Background Ypresian	302-4A (ACEX)	Sluijs et al. (2006)
8	10	83.2	28.85	13.1	24.7	18.0	4.0	Tex_{86}	EECO	302-4A (ACEX)	Sluijs et al. (2006)
9	11	38.0	-56.12	25.6	27.4	23.7	2.3	Tex_{86} and Foram. $\delta^{18}O$	Earliest Eocene	Bass River, USA	John et al. (2008); Sluijs et al. (2007)
10	12	38.2	-56.69	25.6	26.7	24.1	4.0	Tex_{86}	Earliest Eocene	Wilson Lake, USA	Zachos et al. (2007)
11	13	5.5	-143.9	29.4	30.1	28.5	1.1	Mg/Ca	Earliest Eocene	ODP 865	Tripati & Elderfield (2004)
12	14	-31.1	-7.38	27.4	28.1	26.7	1.1	Mg/Ca	Earliest Eocene	DSDP 527	Tripati & Elderfield (2004)
13	15	22.0	-162	28.1	28.4	27.8	1.1	Mg/Ca	Earliest Eocene	ODP 1209	Zachos et al. (2003)

Table 3 – Summary of 15 marine proxy data points used for marine model-data comparison. The original data set (19 data points) was compiled in Lunt et al., (2012) from 13 locations. We have taken the mean temperature value from different proxy methods at each location but have not calculated means for data of different ages.

ID	MAT (°C)	RHCRIT	VF1	CT	CW_LAND	CW_SEA	Z0FSEA	KAY_GWAVE	ALPHAM	ATM_DIFF	OCN_DIFF_H	OCN_DIFF_V
E1	12.3	100	73	67	754	787	429	86	312	99	103	98
E2	14.9	107	75	75	807	843	353	88	221	89	98	83
E3	15.2	107	52	77	1113	1169	167	69	132	97	105	88
E4	15.9	91	40	60	562	583	161	78	189	99	102	85
E5	16.9	117	88	71	630	655	376	91	182	85	87	98
E6	17.6	106	67	53	118	112	198	82	205	95	97	83
E7	20.8	101	107	195	1098	1152	100	88	286	87	89	86
E8	21.1	113	102	124	971	1018	328	94	239	90	90	82
E9	21.1	109	91	117	992	1040	135	67	306	94	89	99
E10	21.2	117	104	99	771	805	439	55	309	88	89	86
E11	22.1	91	111	313	1201	1262	209	61	153	86	104	91
E12	24.6	89	42	135	909	951	401	81	202	99	85	90
E13	25.0	89	65	248	1017	1067	305	68	265	96	104	98
E14	25.3	89	100	100	10	100	100	100	100	100	100	100
E15	26.3	92	49	212	1210	1272	349	87	165	93	102	99
E16	29.7	100	100	100	10	100	100	93	100	100	100	100
E17	31.8	95	108	321	1050	1102	108	100	108	97	99	92
E6000	na	89	90	309	379	389	25	93	214	86	102	82

Table 4 – Parameter values of the final 17 Eocene simulations as a percentage of the original standard parameter value (for standard parameter value see table 1). Simulations are ranked in order of lowest to highest mean annual temperatures (MAT, also shown), i.e. simulation E1 has the coolest MAT and E17 has the warmest MAT. The parameter values of simulation E6000 on which the single parameter perturbations were based on are also included for reference, although note that this simulations is not part of the final 17 Eocene simulations.

ID	MAT (°C)	Tropical SSTs (°C)	NH polar SSTs (°C)	SH polar SSTs (°C)	Tropical terr. temp. (°C)	NH polar terr. temp. (°C)	SH polar terr. temp. (°C)	NH SST EPTD (°C)	SH SST EPTD (°C)	NH terr. EPTD (°C)	SH terr. EPTD (°C)	MAP (mm/day)	Surface albedo (%)	Planetary albedo (%)	Low cloud (%)	High cloud (%)	Totalcloud (%)	Net solar radiation toa (Wm^{-2})
PD	14.5	27.9	0.8	0.1	27.0	-8.9	-6.6	27.2	27.8	35.8	33.6	2.9	13.9	33.1	23.7	23.4	52.4	235.4
E1	12.3	23.9	-1.2	-0.7	25.3	-18.2	-17.3	25.1	24.6	43.5	42.7	2.7	14.8	35.4	28.5	25.2	57.3	227.6
E2	14.9	26.0	-0.6	0.4	27.6	-13.7	-12.7	26.5	25.6	41.3	40.3	2.8	12.0	34.2	27.5	26.2	56.1	231.8
E3	15.2	26.0	-0.6	0.4	38.2	-1.0	-0.3	26.5	25.6	39.2	38.5	2.8	11.2	35	28.5	29.1	58.6	228.8
E4	15.9	26.6	-0.2	0.9	27.9	-11.5	-11.2	26.8	25.7	39.4	39.1	2.8	11.2	35.3	28.8	29.6	60	227.3
E5	16.9	27.7	0.2	1.3	29.8	-10.1	-10.4	27.5	26.4	39.9	40.2	3.0	10.8	33.2	26.4	26.7	54.3	235.6
E6	17.6	28.0	0.6	1.7	30.0	-8.4	-9.4	27.4	26.3	38.4	39.4	3.0	10.5	32.8	25.6	25.9	54.3	236.0
E7	20.8	32.1	0.9	3.1	33.7	-7.4	-6.0	31.2	29.0	41.1	39.7	3.3	10.3	30.9	22.7	22.5	49.3	243.6
E8	21.1	32.2	0.9	3.5	34.6	-6.7	-5.3	31.3	28.8	41.2	39.9	3.4	10.0	31.3	23.4	24.5	49.9	242.7
E9	21.1	32.3	0.0	6.2	34.0	-9.5	-2.0	32.2	26.0	43.5	36.1	3.3	10.3	31.3	22.9	24.3	49.9	242.5
E10	21.2	32.3	0.9	3.4	34.8	-7.0	-5.3	31.4	28.9	41.8	40.1	3.4	10.3	31.3	23.2	25.1	49.8	243.0
E11	22.1	32.5	2.3	5.0	34.5	-3.8	-3.3	30.2	27.5	38.3	37.8	3.5	9.3	29.8	21.6	20.9	48.4	246.5
E12	24.6	34.9	2.9	6.4	38.2	-1.0	-0.3	31.9	28.5	39.2	38.5	3.4	9.0	32.3	24.3	27.5	55.4	238.2
E13	25	34.8	3.9	7.4	37.9	0.3	0.8	30.9	27.4	37.6	37.2	3.6	8.9	29.5	21.1	22.8	49.8	246.9
E14	25.3	34.1	4.3	13.3	36.7	1.7	6.3	29.8	20.9	34.9	30.4	3.6	8.3	27.8	18.5	20.1	46.2	251.1
E15	26.3	36.4	4.8	8.0	40.2	2.1	1.7	31.6	28.5	38.2	38.6	3.6	8.6	30.9	22.7	25.3	53	242.7
E16	29.7	38.2	11.4	15.2	42.3	9.7	11.0	26.7	22.9	32.5	31.2	3.9	7.7	26.2	16.5	19.7	43.7	256.5
E17	31.8	39.4	14.3	19.3	44.5	12.4	14.5	25.1	20.1	32.0	29.9	4.1	7.6	25.1	15.5	17.3	41.2	259.9

Table 5 – Global mean values for the final 17 Eocene simulations. Tropical mean temperatures are calculated from the mean temperatures between 10°S and 10°N. Polar temperatures are defined between 60° and 90° in each hemisphere (NH = northern hemisphere and SH = southern hemisphere). The Equator to Pole Temperature Gradient (EPTD) for each hemisphere is calculated by subtracting the polar temperatures from the tropical temperatures in each hemisphere.

ID	E1	E2	E3	E4	E5	E6	E7	E8	E9	E10	E11	E12	E13	E14	E15	E16	E17
Entire marine dataset	*16.1*	*14.9*	*14.8*	*14.7*	*14.2*	*14.0*	*12.2*	*12.0*	*11.4*	*12.0*	*10.9*	*10.6*	*10.3*	*8.9*	*10.0*	*8.1*	***7.9***
Earliest Eocene data	8.0	6.0	6.1	5.3	4.8	4.1	2.2	2.5	2.8	2.7	**1.9**	2.7	2.7	2.2	3.5	5.1	6.4
Background early Eocene data	15.9	15.0	14.8	14.6	14.3	14.0	12.7	12.5	11.9	12.5	11.4	11.2	10.9	9.7	10.6	**8.8**	9.4
EECO data	24.5	23.0	23.0	23.2	22.2	22.0	19.0	18.5	17.6	18.4	16.9	16.0	15.4	12.9	14.7	9.9	**6.2**
Antarctic ocean data	17.0	15.0	15.3	15.0	14.0	13.5	9.6	9.2	7.8	9.0	7.7	6.0	5.5	**5.2**	5.2	7.7	9.2
Pacific ocean data	18.2	17.3	17.1	17.0	16.5	16.4	14.6	14.2	13.4	14.2	12.9	12.6	12.1	9.5	11.9	9.3	**8.2**
Atlantic ocean data	8.1	6.2	6.0	5.5	5.1	4.3	2.1	2.5	3.0	2.7	1.7	2.0	2.0	**1.3**	2.1	3.5	5.4
Arctic ocean data	20.0	19.8	19.6	19.7	19.7	19.6	19.8	19.7	19.9	19.8	18.9	19.0	18.8	17.5	18.2	11.3	**8.5**
Late Paleocene and background early Eocene data	13.2	12.1	12.0	11.7	11.4	11.0	9.8	9.7	9.3	9.7	8.8	8.7	8.5	7.5	8.4	**7.5**	8.3
Entire terrestrial dataset	*21.6*	*18.8*	*18.1*	*17.1*	*16.3*	*14.9*	*12.9*	*12.9*	*14.0*	*12.9*	*11.0*	*8.8*	*8.0*	*7.7*	*7.0*	***4.8***	*5.1*
Terrestrial SH polar region	22.6	19.2	18.5	17.9	17.0	16.1	12.4	12.0	10.8	12.0	10.7	7.9	7.2	5.3	6.7	**3.7**	5.5
Terrestrial SH mid latitudes	18.6	15.2	15.2	14.7	13.7	12.8	9.8	9.3	8.8	9.2	8.5	6.3	5.8	4.9	5.4	**3.7**	5.5
Terrestrial NH polar region	18.5	16.8	16.3	15.0	14.4	12.9	10.6	10.9	11.9	10.8	9.1	7.0	6.3	6.8	5.6	**4.8**	5.2
Terrestrial NH mid latitudes	33.3	27.9	26.1	25.8	24.1	22.5	22.1	21.5	24.4	21.8	18.5	15.7	14.8	13.1	12.3	5.8	**4.1**
Entire marine and terrestrial dataset	*20.5*	*18.0*	*17.4*	*16.6*	*15.8*	*14.7*	*12.7*	*12.7*	*13.4*	*12.7*	*11.0*	*9.2*	*8.6*	*8.0*	*7.8*	***5.7***	*5.9*

Table 6 - Root mean square error (RMSE) calculations for differences between simulation temperature predictions and proxy data temperature estimates. RMSE has been calculated for the entire combined terrestrial and marine proxy dataset and the separated marine and terrestrial data sets (highlighted in grey). RMSE are also calculated for each subdivision of age in the marine data: Earliest Eocene (~55 Ma), Early Eocene Climatic Optimum (EECO) and Ypresian. RMSE for different geographical subsets of terrestrial data have also been calculated. The minimum RMSE for each group and subgroup is highlighted in bold. All simulation estimates are calculated from a grid box mean centred over the proxy data points' paleolocation.

Figure 1 - Annual surface air temperature for (a) the coolest simulation E1 and (b) the warmest simulation E17 from the final Eocene ensemble

Figure 2 - Seasonal (DJF, JJA) precipitation for (a) & (b) the coolest simulation E1 and (c) & (d) the warmest simulation E17 from the final Eocene ensemble

Figure 3 - Atlantic meridional streamfunction (Sv) for the present day (PD) and final ensemble of 17 Eocene models. Positive values indicate clockwise motion and negative values indicate anticlockwise motion.

Figure 4 – Early Eocene sea surface temperatures (SSTs) as compiled in Lunt et al., (2012) shown as solid black circles. Upper and lower temperature error bars are shown in black and calibration errors are plotted in grey. Simulated zonal SSTs are plotted over the top. The four warmest simulations: E14 (solid red line); E15 (dotted purple line); E16 (dashed black line) and E17 (dotted blue line) are highlighted with thicker lines for clarity.

Figure 5 – Early Eocene terrestrial MATs as compiled in Huber & Cabellero (2011) shown as solid black circles. Upper and lower temperature error bars are shown in black and calibration errors are plotted in grey. Simulated terrestrial zonal mean temperatures are plotted over the top. The four warmest simulations: E14 (solid red line); E15 (dotted purple line); E16 (dashed black line) and E17 (dotted blue line) are highlighted with thicker lines for clarity.

Figure 6 - Histogram showing error (simulation temperature estimate minus proxy data temperature) for all terrestrial data points. Note that 0 is not in the centre of the x axis. Number above graph denotes rank of simulation in terms of MAT.

Figure 7 - Histogram showing error (simulation temperature estimate minus proxy data temperature) for all marine data points. Note that 0 is not in the centre of the x axis. Number above graph denotes rank of simulation in terms of MAT.

Figure 8 – Ocean, atmosphere and heat transport in four warmest simulations (E14-E17) and present day (PD) control simulation for each hemisphere plotted against latitude

Figure 9 – Ocean heat transport (OHT) calculated as a percent of total heat transport in each hemisphere for the Eocene simulations and plotted against a) Tropical sea surface temperatures (SSTs) b) Equator to pole temperature difference (EPTD). Northern hemisphere data plotted in blue and southern hemisphere data plotted in red. R^2 correlation coefficients also shown.

References

1. Barron EJ. A warm, equable Cretaceous: the nature of the problem. Earth-Science Reviews. 1983;19(4):305–38.

2. Frakes LA, Francis JE. A guide to Phanerozoic cold polar climates from high-latitude ice-rafting in the Cretaceous. 1988

3. Huber M, Caballero R. The early Eocene equable climate problem revisited. Climate of the Past. 2011;7:603–33.

4. Lunt DJ, Jones TD, Heinemann M, Huber M, LeGrande A, Winguth A, et al. A model-data comparison for a multi-model ensemble of early Eocene atmosphere-ocean simulations: EoMIP. Climate of the Past 2012; 8, 1717-1736,

5. Spicer RA, Valdes PJ, Spicer TEV, Craggs HJ, Srivastava G, Mehrotra RC, et al. New developments in CLAMP: Calibration using global gridded meteorological data. Palaeogeography, palaeoclimatology, palaeoecology. 2009;283(1-2):91–8.

6. Winguth AME, Thomas E, Winguth C. Global decline in ocean ventilation, oxygenation, and productivity during the Paleocene-Eocene Thermal Maximum: Implications for the benthic extinction. Geology. 2012;40(3):263–6.

7. Sluijs A, Schouten S, Pagani M, Woltering M, Brinkhuis H, DamstÃ JSS, et al. Subtropical Arctic Ocean temperatures during the Palaeocene/Eocene thermal maximum. Nature. 2006;441(7093):610–3.

8. Weijers JWH, Schouten S, Sluijs A, Brinkhuis H, Sinninghe Damsté JS. Warm arctic continents during the Palaeocene-Eocene thermal maximum. Earth and Planetary Science Letters. 2007;261(1-2):230–8.

9. Ivany LC, Lohmann KC, Hasiuk F, Blake DB, Glass A, Aronson RB, et al. Eocene climate record of a high southern latitude continental shelf: Seymour Island, Antarctica. Geological Society of America Bulletin. 2008;120(5-6):659–78.

10. Stott LD, Kennett JP, Shackleton NJ, Corfield RM. 48. The evolution of antarctic surface waters during the paleogene: inferences from the stable isotopic composition of planktonic foraminifers, odp leg 1131. Proc Ocean Drilling Project Sci Results. 1990;113:849–63.

11. Bijl PK, Schouten S, Sluijs A, Reichart GJ, Zachos JC, Brinkhuis H. Early Palaeogene temperature evolution of the southwest Pacific Ocean. Nature. 2009;461(7265):776–9.

12. Greenwood DR, Moss PT, Rowett AI, Vadala AJ, Keefe RL. Plant communities and climate change in southeastern Australia during the early Paleogene. Special papers-geological society of America. 2003;365–80.

13. Greenwood DR, Wilf P, Wing SL, Christophel DC. Paleotemperature estimation using leaf-margin analysis: Is Australia different? Palaios. 2004;19 (2):129–42.

14. Hunt RJ, Poole I. Paleogene West Antarctic climate and vegetation history in light of new data from King George Island. Special papers-geological society of America. 2003;395–412.

15. Pearson PN, Van Dongen BE, Nicholas CJ, Pancost RD, Schouten S, Singano JM, et al. Stable warm tropical climate through the Eocene Epoch. Geology. 2007;35(3):211.

16. Pagani M, Pedentchouk N, Huber M, Sluijs A, Schouten S, Brinkhuis H, et al. Arctic hydrology during global warming at the Palaeocene/Eocene thermal maximum. Nature. 2006;442(7103):671–5.

17. Bowen GJ, Beerling DJ, Koch PL, Zachos JC, Quattlebaum T. A humid climate state during the Palaeocene/Eocene thermal maximum. Nature. 2004 Nov 25;432(7016):495–9.

18. Tripati AK, Elderfield H. Abrupt hydrographic changes in the equatorial Pacific and subtropical Atlantic from foraminiferal Mg/Ca indicate greenhouse origin for the thermal maximum at the Paleocene-Eocene Boundary. Geochem. Geophys. Geosyst. 2004 Feb 14;5(2):Q02006.

19. Pierrehumbert RT. The hydrologic cycle in deep-time climate problems. Nature. 2002 Sep 12;419(6903):191–8.

20. Barron EJ. Eocene equator-to-pole surface ocean temperatures: A significant climate problem? Paleoceanography. 1987;2(6):729–39.

21. Pearson PN, Ditchfield PW, Singano J, Harcourt-Brown KG, Nicholas CJ, Olsson RK, et al. Warm tropical sea surface temperatures in the Late Cretaceous and Eocene epochs. Nature. 2001;413(6855):481–7.

22. Greenwood DR. Leaf form and the reconstruction of past climates. New Phytologist. 2005;166(2):355–7.

23. Kowalski EA. Mean annual temperature estimation based on leaf morphology: a test from tropical South America. Palaeogeography, Palaeoclimatology, Palaeoecology. 2002;188(3):141–65.

24. Kowalski EA, Dilcher DL. Warmer paleotemperatures for terrestrial ecosystems. Proceedings of the National Academy of Sciences. 2003;100(1):167–70.

25. Peppe DJ, Royer DL, Wilf P, Kowalski EA. Quantification of large uncertainties in fossil leaf paleoaltimetry. Tectonics. 2010;29(3):TC3015.

26. Sloan LC, Barron EJ. ‘ Equable’ climates during Earth history? Geology. 1990;18(6):489–92.

27. Sloan LC, Barron EJ. A comparison of Eocene climate model results to quantified paleoclimatic interpretations. Palaeogeography, Palaeoclimatology, Palaeoecology. 1992;93(3-4):183–202.

28. Kirk-Davidoff DB, Schrag DP, Anderson JG. On the feedback of stratospheric clouds on polar climate. Geophysical research letters. 2002;29(11):51–1.

29. Emanuel K. A simple model of multiple climate regimes. J. Geophys. Res [Internet]. 2002;107(0).

30. Emanuel K, DesAutels C, Holloway C, Korty R. Environmental control of tropical cyclone intensity. Journal of the atmospheric sciences. 2004;61(7):843–58.

31. Korty RL, Emanuel KA, Scott JR. Tropical cyclone-induced upper-ocean mixing and climate: Application to equable climates. Journal of Climate. 2008;21(4):638–54.

32. Sloan LC. Equable climates during the early Eocene: Significance of regional paleogeography for North American climate. Geology. 1994;22(10):881–4.

33. Sloan LC, Huber M. Eocene oceanic responses to orbital forcing on precessional time scales. Paleoceanography. 2001;16(1):101–11.

34. Sloan LC, Morrill C. Orbital forcing and Eocene continental temperatures. Palaeogeography, Palaeoclimatology, Palaeoecology. 1998;144(1):21–35.

35. Huber M, Brinkhuis H, Stickley CE, Doos K, Sluijs A, Warnaar J, et al. Eocene circulation of the Southern Ocean: Was Antarctica kept warm by subtropical waters. Paleoceanography. 2004;19(4):PA4026.

36. Huber M, Nof D. The ocean circulation in the southern hemisphere and its climatic impacts in the Eocene. Palaeogeography, Palaeoclimatology, Palaeoecology. 2006;231(1):9–28.

37. Sloan LC, Huber M, Ewing A. Polar stratospheric cloud forcing in a greenhouse world. Reconstructing ocean history: a window into the future. 1999;273:293.

38. Kirk-Davidoff DB, Lamarque JF. Maintenance of polar stratospheric clouds in a moist stratosphere. Climate of the Past Discussions. 2007;3(4):935–60.

39. Abbot DS, Tziperman E. A high-latitude convective cloud feedback and equable climates. Quarterly Journal of the Royal Meteorological Society. 2008;134(630):165–85.

40. Abbot DS, Tziperman E. Sea ice, high-latitude convection, and equable climates. Geophys. Res. Lett. 2008;35(L03702):L03702.

41. Kump LR, Pollard D. Amplification of Cretaceous warmth by biological cloud feedbacks. Science. 2008;320(5873):195–195.

42. Andreae MO. Aerosols before pollution. Science(Washington). 2007;315(5808):50–1.

43. Heinemann M, Jungclaus JH, Marotzke J. Warm Paleocene/Eocene climate as simulated in ECHAM5/MPI-OM. Climate Past. 2009;5:785–802.

44. Roberts CD, LeGrande AN, Tripati AK. Climate sensitivity to Arctic seaway restriction during the early Paleogene. Earth and Planetary Science Letters. 2009 Sep;286(3-4):576–85.

45. Liu Z, Pagani M, Zinniker D, DeConto R, Huber M, Brinkhuis H, et al. Global cooling during the Eocene-Oligocene climate transition. Science. 2009;323(5918):1187–90.

46. Winguth A, Shellito C, Shields C, Winguth C. Climate Response at the Paleocene–Eocene Thermal Maximum to Greenhouse Gas Forcing—A Model Study with CCSM3. Journal of Climate. 2010 May;23(10):2562–84.

47. Hollis CJ, Handley L, Crouch EM, Morgans HEG, Baker JA, Creech J, et al. Tropical sea temperatures in the high-latitude South Pacific during the Eocene. Geology. 2009;37(2):99–102.

48. McGuffie K, Henderson-Sellers A. A Climate Modelling Primer. 3rd ed. Wiley; 2005.

49. Murphy JM, Sexton DMH, Barnett DN, Jones GS, Webb MJ, Collins M, et al. Quantification of modelling uncertainties in a large ensemble of climate change simulations. Nature. 2004;430(7001):768–72.

50. Tebaldi C, Knutti R. The use of the multi-model ensemble in probabilistic climate projections. Phil. Trans. R. Soc. A. 2007 Aug 15;365(1857):2053–75.

51. Cubasch U, Meehl GA, Boer GJ, Stouffer RJ, Dix M, Noda A, et al. Projections of future climate change. , in: JT Houghton, Y. Ding, DJ Griggs, M. Noguer, PJ Van der Linden, X. Dai, K. Maskell, and CA Johnson (eds.): Climate Change 2001: The Scientific Basis: Contribution of Working Group I to the Third Assessment Report of the Intergovernmental Panel. 2001;526–82.

52. Stainforth DA, Aina T, Christensen C, Collins M, Faull N, Frame DJ, et al. Uncertainty in predictions of the climate response to rising levels of greenhouse gases. Nature. 2005;433(7024):403–6.

53. Mikolajewicz U, Groger M, Maier-Reimer E, Schurgers G, Vizcaino M, Winguth AME. Long-term effects of anthropogenic CO2 emissions simulated with a complex earth system model. Climate Dynamics. 2007;28(6):599–634.

54. Sexton DMH, Murphy JM, Collins M, Webb MJ. Multivariate probabilistic projections using imperfect climate models part I: outline of methodology. Climate Dynamics. 2011;1–30.

55. Schneider von Deimling T, Held H, Ganopolski A, Rahmstorf S. Climate sensitivity estimated from ensemble simulations of glacial climate. Climate Dynamics. 2006;27(2):149–63.

56. Schmittner A, Silva TAM, Fraedrich K, Kirk E, Lunkeit F. Effects of Mountains and Ice Sheets on Global Ocean Circulation. Journal of Climate. 2011 Jun;24(11):2814–29.

57. Hargreaves JC, Abe-Ouchi A, Annan JD, others. Linking glacial and future climates through an ensemble of GCM simulations. Climate of the Past. 2007;3(1):77–87.

58. Hargreaves JC, Annan JD. On the importance of paleoclimate modelling for improving predictions of future climate change. Climate of the Past 5(4)

59. Brown J, Collins M, Tudhope AW, Toniazzo T. Modelling mid-Holocene tropical climate and ENSO variability: towards constraining predictions of future change with palaeo-data. Climate Dynamics. 2008;30(1):19–36.

60. Gregoire LJ, Valdes PJ, Payne AJ, Kahana R. Optimal tuning of a GCM using modern and glacial constraints. Climate dynamics. 2011;37(3):705–19.

61. Pope JO, Collins M, Haywood AM, Dowsett HJ, Hunter SJ, Lunt DJ, et al. Quantifying uncertainty in model predictions for the Pliocene (Plio-QUMP): initial results. Palaeogeography, Palaeoclimatology, Palaeoecology [Internet]. 2011

62. Jones C, Gregory J, Thorpe R, Cox P, Murphy J, Sexton D, et al. Systematic optimisation and climate simulation of FAMOUS, a fast version of HadCM3. Climate dynamics. 2005;25(2):189–204.

63. Gordon C, Cooper C, Senior CA, Banks H, Gregory JM, Johns TC, et al. The simulation of SST, sea ice extents and ocean heat transports in a version of the Hadley Centre coupled model without flux adjustments. Climate Dynamics. 2000;16(2):147–68.

64. Smith RS, Gregory JM, Osprey A, others. A description of the FAMOUS (version XDBUA) climate model and control run. Geoscientific Model Development. 2008;1(1):53–68.

65. Pope VD, Gallani ML, Rowntree PR, Stratton RA. The impact of new physical parametrizations in the Hadley Centre climate model: HadAM3. Climate Dynamics. 2000;16(2):123–46.

66. Cox PM, Betts RA, Bunton CB, Essery RLH, Rowntree PR, Smith J. The impact of new land surface physics on the GCM simulation of climate and climate sensitivity. Climate Dynamics. 1999;15(3):183–203.

67. Randall DA, Wood RA, Bony S, Colman R, Fichefet T, Fyfe J, et al. Cilmate Models and Their Evaluation. In: Climate Change 2007: The Physical Science Basis. Contribution of Working Group I to the Fourth Assessment Report of the Intergovernmental Panel on Climate Change. Cambridge University Press, Cambridge, United Kingdom and New York, NY, USA. 2007;

68. Ziegler AM, Rowley DB, Lottes AL, Sahagian DL, Hulver ML, Gierlowski TC. Paleogeographic Interpretation: With an Example From the Mid-Cretaceous. Annual Review of Earth and Planetary Sciences. 1985;13(1):385–428.

69. Ziegler AM. Models come in from the cold. , Published online: 07 January 1993; | doi:10.1038/361016a0. 1993 Jan 7;361(6407):16–7.

70. Yemane K. Contribution of Late Permian palaeogeography in maintaining a temperate climate in Gondwana. , Published online: 07 January 1993; | doi:10.1038/361051a0. 1993 Jan 7;361(6407):51–4.

71. Markwick PJ, Valdes PJ. Palaeo-digital elevation models for use as boundary conditions in coupled ocean–atmosphere GCM experiments: a Maastrichtian (late Cretaceous) example. Palaeogeography, Palaeoclimatology, Palaeoecology. 2004;213(1):37–63.

72. Sewall J.O., Sloan L.C., Huber M., Wing S. Climate sensitivity to changes in land surface characteristics. Global and Planetary Change. 2000;26(4):445–65.

73. Hoskins BJ, Karoly DJ. The steady linear response of a spherical atmosphere to thermal and orographic forcing. Journal of the Atmospheric Sciences. 1981;38(6):1179–96.

74. Kutzbach JE, Prell WL, Ruddiman WF. Sensitivity of Eurasian Climate to Surface Uplift of the Tibetan Plateau. The Journal of Geology. 1993 Mar 1;101(2):177–90.

75. Wilson C, Sinha B, Williams RG. The shaping of storm tracks by mountains and ocean dynamics. Weather. 2010;65(12):320–3.

76. Tindall J, Flecker R, Valdes P, Schmidt DN, Markwick P, Harris J. Modelling the oxygen isotope distribution of ancient seawater using a coupled ocean-atmosphere GCM: implications for reconstructing early Eocene climate. Earth and Planetary Science Letters. 2010;292(3-4):265–73.

77. Royer DL, Wing SL, Beerling DJ, Jolley DW, Koch PL, Hickey LJ, et al. Paleobotanical Evidence for Near Present-Day Levels of Atmospheric CO2 During Part of the Tertiary. Science. 2001 Jun 22;292(5525):2310–3.

78. Retallack GJ. Carbon dioxide and climate over the past 300 Myr. Philosophical Transactions of the Royal Society of London. Series A: Mathematical, Physical and Engineering Sciences. 2002;360(1793):659–73.

79. Yapp CJ. Fe (CO3) OH in goethite from a mid-latitude North American Oxisol: estimate of atmospheric CO2 concentration in the Early Eocene. Geochimica et Cosmochimica Acta. 2004;68(5):935–47.

80. Beerling DJ, Royer DL. Convergent Cenozoic CO2 history. Nature Geoscience. 2011;4(7):418–20.

81. Pagani M, Zachos JC, Freeman KH, Tipple B, Bohaty S. Marked decline in atmospheric carbon dioxide concentrations during the Paleogene. Science. 2005;309(5734):600–3.

82. Sloan LC, Walker JCG, Moore TC, Rea DK, Zachos JC. Possible methane-induced polar warming in the early Eocene. 1992

83. DeConto RM, Galeotti S, Pagani M, Tracy D, Schaefer K, Zhang T, et al. Past extreme warming events linked to massive carbon release from thawing permafrost. Nature. 2012 Apr 5;484(7392):87–91.

84. Toney JL, Bendle JA, Seki O, Krishnan S, Pagani M, Inglis G, et al. Insights into peatland expansion and methane cycling on the East Antarctic continent in the early Eocene. EGU General Assembly Conference Abstracts. 2012. p. 8210.

85. Beerling DJ, Fox A, Stevenson DS, Valdes PJ. Enhanced chemistry-climate feedbacks in past greenhouse worlds. Proceedings of the National Academy of Sciences. 2011; 108(24):9770–5.

86. Laskar J, Robutel P, Joutel F, Gastineau M, Correia ACM, Levrard B. A long-term numerical solution for the insolation quantities of the Earth. Astronomy and Astrophysics. 2004 Dec;428(1):261–85.

87. Lourens LJ, Sluijs A, Kroon D, Zachos JC, Thomas E, Röhl U, et al. Astronomical pacing of late Palaeocene to early Eocene global warming events. Nature. 2005 Jun 8;435(7045):1083–7.

88. Westerhold T, Röhl U, Laskar J, Raffi I, Bowles J, Lourens LJ, et al. On the duration of magnetochrons C24r and C25n and the timing of early Eocene global warming events: Implications from the Ocean Drilling Program Leg 208 Walvis Ridge depth transect. Paleoceanography. 2007;22(2)

89. Galeotti S, Krishnan S, Pagani M, Lanci L, Gaudio A, Zachos JC, et al. Orbital chronology of Early Eocene hyperthermals from the Contessa Road section, central Italy. Earth and Planetary Science Letters. 2010;290(1):192–200.

90. Lunt DJ, Ridgwell A, Sluijs A, Zachos J, Hunter S, Haywood A. A model for orbital pacing of methane hydrate destabilization during the Palaeogene. Nature Geoscience. 2011

91. Bonan GB, Pollard D, Thompson SL. Effects of boreal forest vegetation on global climate. doi:10.1038/359716a0. 1992 Oct 22;359(6397):716–8.

92. Henderson-Sellers A, Dickinson RE, Durbidge TB, Kennedy PJ, McGuffie K, Pitman AJ. Tropical deforestation: Modeling local- to regional-scale climate change. Journal of Geophysical Research: Atmospheres. 1993;98(D4):7289–315.

93. Foley JA, Kutzbach JE, Coe MT, Levis S. Feedbacks between climate and boreal forests during the Holocene epoch. doi:10.1038/371052a0. 1994 Sep 1;371(6492):52–4.

94. Shellito CJ, Sloan LC. Reconstructing a lost Eocene paradise: Part I. Simulating the change in global floral distribution at the initial Eocene thermal maximum. Global and Planetary Change. 2006 Feb;50(1–2):1–17.

95. Shellito CJ, Sloan LC. Reconstructing a lost Eocene Paradise, Part II: On the utility of dynamic global vegetation models in pre-Quaternary climate studies. Global and Planetary Change. 2006 Feb;50(1–2):18–32.

96. Peng C. From static biogeographical model to dynamic global vegetation model: a global perspective on modelling vegetation dynamics. Ecological Modelling. 2000 Nov 25;135(1):33–54.

97. Betts RA. Self-beneficial effects of vegetation on climate in an ocean-atmosphere general circulation model. Geophysical Research Letters. 1999;26(10):1457–60.

98. McKay MD. Latin hypercube sampling as a tool in uncertainty analysis of computer models. Proceedings of the 24th conference on Winter simulation. 1992. p. 557–64.

99. Loeppky JL, Sacks J, Welch WJ. Choosing the sample size of a computer experiment: A practical guide. Technometrics. 2009;51(4):366–76.

100. Harrison T, Msuya CP, Murray AM, Jacobs BF, Baez AM, Ludwig KR, et al. Paleontological investigations at the Eocene locality of Mahenge in north-central Tanzania, East Africa. Eocene Biodiversity: Unusual Occurrences and Rarely Sampled Habitats. Kluwer/Plenum, New York. 2001;39–74.

101. Jacobs BF. Palaeobotanical studies from tropical Africa: relevance to the evolution of forest, woodland and savannah biomes. Phil. Trans. R. Soc. Lond. B. 2004 Oct 29;359(1450):1573–83.

102. Müller RD, Sdrolias M, Gaina C, Steinberger B, Heine C. Long-term sea-level fluctuations driven by ocean basin dynamics. science. 2008;319(5868):1357–62.

103. Hren MT, Pagani M, Erwin DM, Brandon M. Biomarker reconstruction of the early Eocene paleotopography and paleoclimate of the northern Sierra Nevada. Geology. 2010 Jan 1;38(1):7–10.

104. Zachos JC, Dickens GR, Zeebe RE. An early Cenozoic perspective on greenhouse warming and carbon-cycle dynamics. Nature. 2008 Jan 17;451(7176):279–83.

105. Roberts CD, LeGrande AN, Tripati AK. Sensitivity of seawater oxygen isotopes to climatic and tectonic boundary conditions in an early Paleogene simulation with GISS ModelE-R. Paleoceanography 2011

106. Keating-Bitonti CR, Ivany LC, Affek HP, Douglas P, Samson SD. Warm, not super-hot, temperatures in the early Eocene subtropics. Geology. 2011;39(8):771–4.

107. Schrag DP. Effects of diagenesis on the isotopic record of late paleogene tropical sea surface temperatures. Chemical Geology. 1999 Sep 30;161(1–3):215–24.

108. Emiliani C. Pleistocene temperatures. The Journal of Geology. 1955;538–78.

109. Spero HJ, Bijma J, Lea DW, Bemis BE. Effect of seawater carbonate concentration on foraminiferal carbon and oxygen isotopes. Nature. 1997;390:497–500.

110. Bijma J, Spero HJ, Lea DW. Reassessing foraminiferal stable isotope geochemistry: Impact of the oceanic carbonate system (experimental results). Use of proxies in paleoceanography-Examples from the South Atlantic (G Fischer, G Wefer, eds) Springer, Berlin, Heidelberg. 1999;489–512.

111. Zeebe RE, Sanyal A, Ortiz JD, Wolf-Gladrow DA. A theoretical study of the kinetics of the boric acid–borate equilibrium in seawater. Marine chemistry. 2001;73(2):113–24.

112. Zeebe RE, Bijma J, Hönisch B, Sanyal A, Spero HJ, Wolf-Gladrow DA. Vital effects and beyond: a modelling perspective on developing palaeoceanographical proxy relationships in foraminifera. Geological Society, London, Special Publications. 2008;303(1):45–58.

113. Bice KL, Birgel D, Meyers PA, Dahl KA, Hinrichs KU, Norris RD. A multiple proxy and model study of Cretaceous upper ocean temperatures and atmospheric CO2 concentrations. Paleoceanography. 2006;21(2):PA2002.

114. Schouten S, Hopmans EC, Schefuß E, Sinninghe Damsté JS. Distributional variations in marine crenarchaeotal membrane lipids: a new tool for reconstructing ancient sea water temperatures? Earth and Planetary Science Letters. 2002;204(1):265–74.

115. Kim J-H, Schouten S, Hopmans EC, Donner B, Sinninghe Damsté JS. Global sediment core-top calibration of the TEX86 paleothermometer in the ocean. Geochimica et Cosmochimica Acta. 2008 Feb 15;72(4):1154–73.

116. Schouten S, Forster A, Panoto FE, Sinninghe Damsté JS. Towards calibration of the TEX86 palaeothermometer for tropical sea surface temperatures in ancient greenhouse worlds. Organic Geochemistry. 2007 Sep;38(9):1537–46.

117. Forster PMF, Gregory JM. The climate sensitivity and its components diagnosed from Earth radiation budget data. Journal of climate. 2006;19(1):39–52.

118. Lunt DJ, Valdes PJ, Jones TD, Ridgwell A, Haywood AM, Schmidt DN, et al. CO2-driven ocean circulation changes as an amplifier of Paleocene-Eocene thermal maximum hydrate destabilization. Geology. 2010;38(10):875–8.

119. Caballero R, Huber M. Spontaneous transition to superrotation in warm climates simulated by CAM3. Geophys. Res. Lett. 2010;37(11):L11701.

120. Weijers JWH, Schouten S, Spaargaren OC, Sinninghe Damsté JS. Occurrence and distribution of tetraether membrane lipids in soils: Implications for the use of the TEX86 proxy and the BIT index. Organic Geochemistry. 2006 Dec;37(12):1680–93.

121. Kim JH, Van der Meer J, Schouten S, Helmke P, Willmott V, Sangiorgi F, et al. New indices and calibrations derived from the distribution of crenarchaeal isoprenoid tetraether lipids: Implications for past sea surface temperature reconstructions. Geochimica et Cosmochimica Acta. 2010;74(16):4639–54.

122. Douglas PM, Ivany L, Pagani M, Hollis CJ, Beu AG, Affek HP. Eocene Southern High Latitude Sea Surface Temperatures: New Constraints from Clumped Isotope Paleothermometry. AGU Fall Meeting Abstracts. 2011 Dec;-1:1924.

123. Creech JB, Baker JA, Hollis CJ, Morgans HEG, Smith EGC. Eocene sea temperatures for the mid-latitude southwest Pacific from Mg/Ca ratios in planktonic and benthic foraminifera. Earth and Planetary Science Letters. 2010;299(3):483–95.

124. Lombard F, Labeyrie L, Michel E, Spero HJ, Lea DW. Modelling the temperature dependent growth rates of planktic foraminifera. Marine Micropaleontology. 2009;70(1):1–7.

125. Bijma J, Faber WW, Hemleben C. Temperature and salinity limits for growth and survival of some planktonic foraminifers in laboratory cultures. Journal of Foraminiferal Research. 1990;20(2):95–116.

126. Thompson PR. Planktonic foraminifera in the western north Pacific during the past 150 000 years: comparison of modern and fossil assemblages. Palaeogeography, Palaeoclimatology, Palaeoecology. 1981;35:241–79.

127. Haq BU, Premoli-Silva I, Lohmann GP. Calcareous plankton paleobiogeographic evidence for major climatic fluctuations in the early Cenozoic Atlantic Ocean. Journal of Geophysical Research. 1977;82(27):3861–76.

128. Falkowski PG, Knoll AH. Evolution of primary producers in the sea [Internet]. Elsevier Academic Press; 2007

129. Peters RB, Sloan LC. High concentrations of greenhouse gases and polar stratospheric clouds: A possible solution to high-latitude faunal migration at the latest Paleocene thermal maximum. Geology. 2000;28(11):979.

130. Abbot DS, Huber M, Bousquet G, Walker CC. High-CO2 cloud radiative forcing feedback over both land and ocean in a global climate model. 2009

131. Abbot DS, Walker CC, Tziperman E. Can a Convective Cloud Feedback Help to Eliminate Winter Sea Ice at High CO2 Concentrations? Journal of Climate. 2009;22(21):5719–31.

132. Trenberth KE, Caron JM. Estimates of meridional atmosphere and ocean heat transports. Journal of Climate. 2001;14(16):3433–43.

133. Rind D, Chandler M. Increased ocean heat transports and warmer climate. Journal of Geophysical Research. 1991;96(D4):7437–61.

134. Solomon S. Climate change 2007: contribution of working group I to the fourth assessment report of the intergovernmental panel on climate change. Cambridge University Press; 2007.

135. DeConto RM, Pollard D. A coupled climate–ice sheet modeling approach to the early Cenozoic history of the Antarctic ice sheet. Palaeogeography, Palaeoclimatology, Palaeoecology. 2003;198(1):39–52.

136. DeConto RM, Pollard D. Rapid Cenozoic glaciation of Antarctica induced by declining atmospheric CO 2. Nature. 2003;421(6920):245–9.

137. Valdes P. Built for stability. Nature Geoscience. 2011;4(7):414–6.

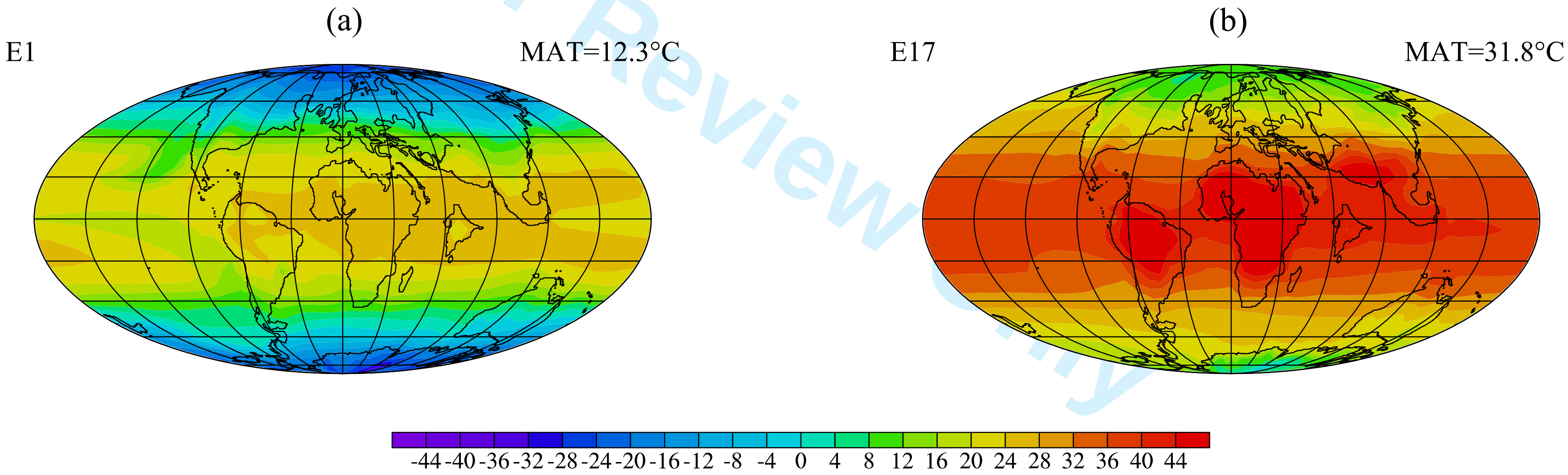
(a)
E1
MAT=12.3°C
(b)
E17
MAT=31.8°C
-44 -40 -36 -32 -28 -24 -20 -16 -12 -8 -4 0 4 8 12 16 20 24 28 32 36 40 44

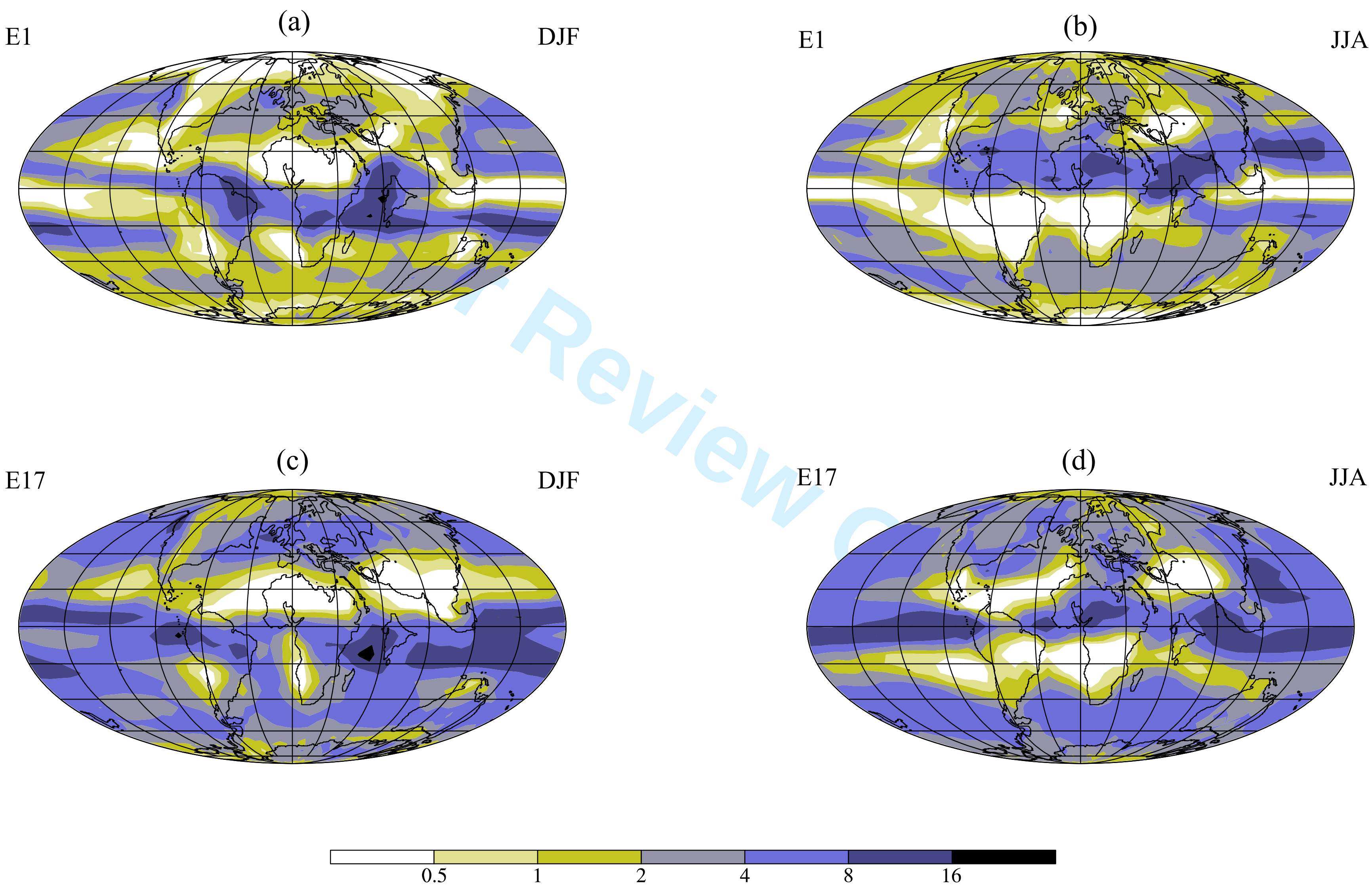
E1
(a)
DJF
E1
(b)
JJA
E17
(c)
DJF
E17
(d)
JJA
0.5
1
2
4
8
16

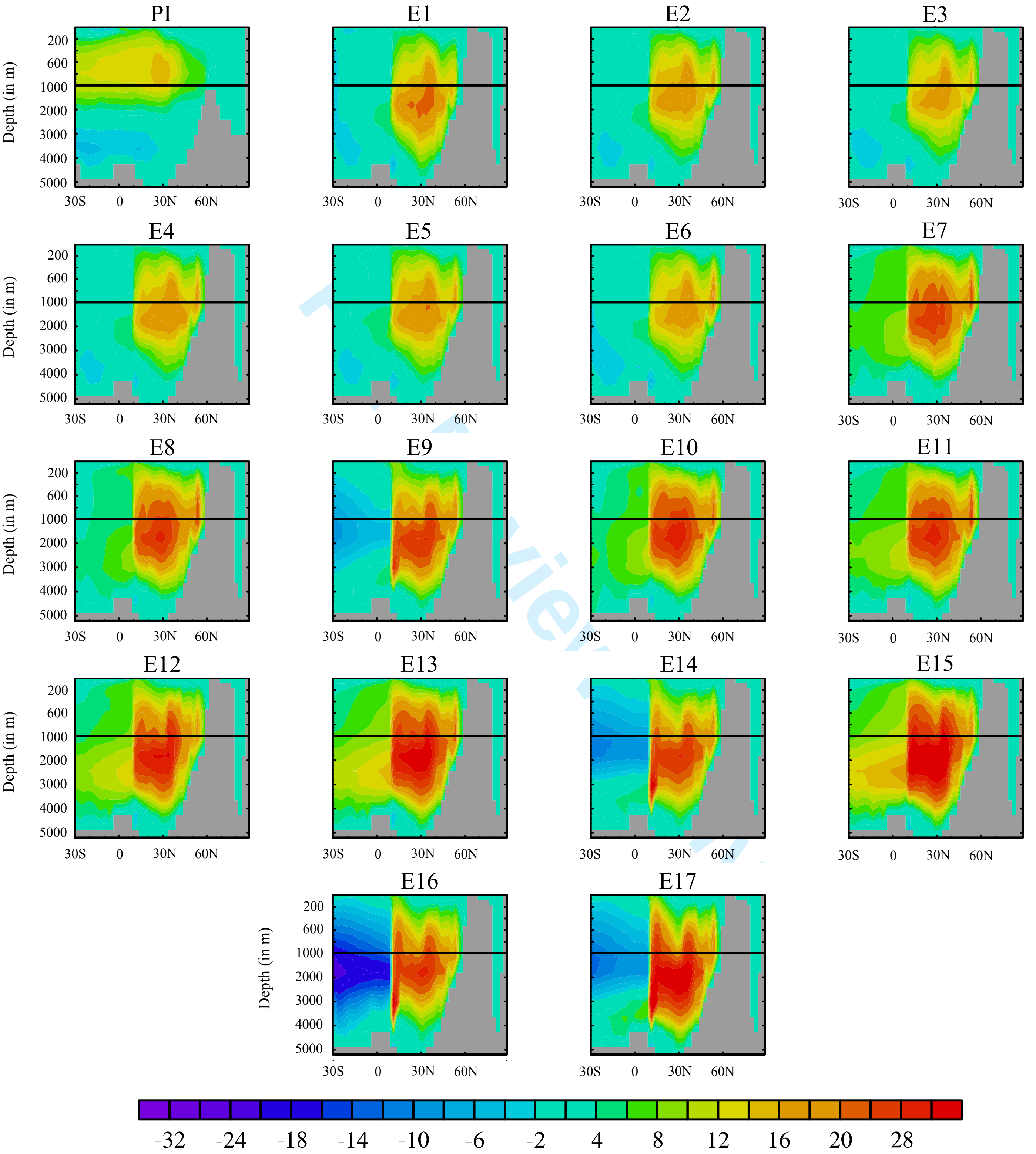
PI
E1
E2
E3
E4
E5
E6
E7
E8
E9
E10
E11
E12
E13
E14
E15
E16
E17
Depth (in m)
200
600
1000
2000
3000
4000
5000
30S
0
30N
60N
-32
-24
-18
-14
-10
-6
-2
4
8
12
16
20
28

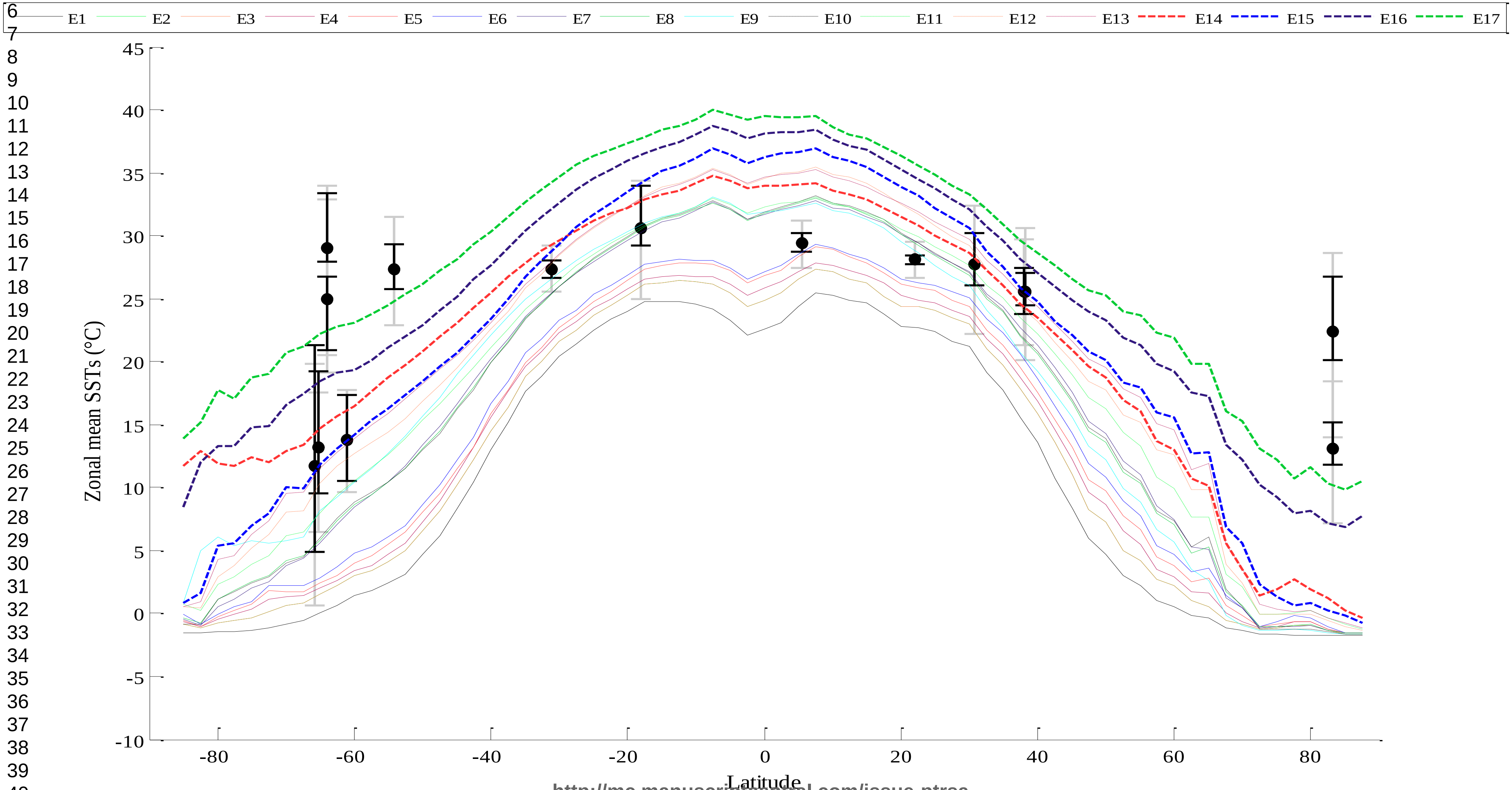
E1
E2
E3
E4
E5
E6
E7
E8
E9
E10
E11
E12
E13
E14
E15
E16
E17
Zonal mean SSTs (°C)
45
40
35
30
25
20
15
10
5
0
-5
-10
-80
-60
-40
-20
0
20
40
60
80
Latitude

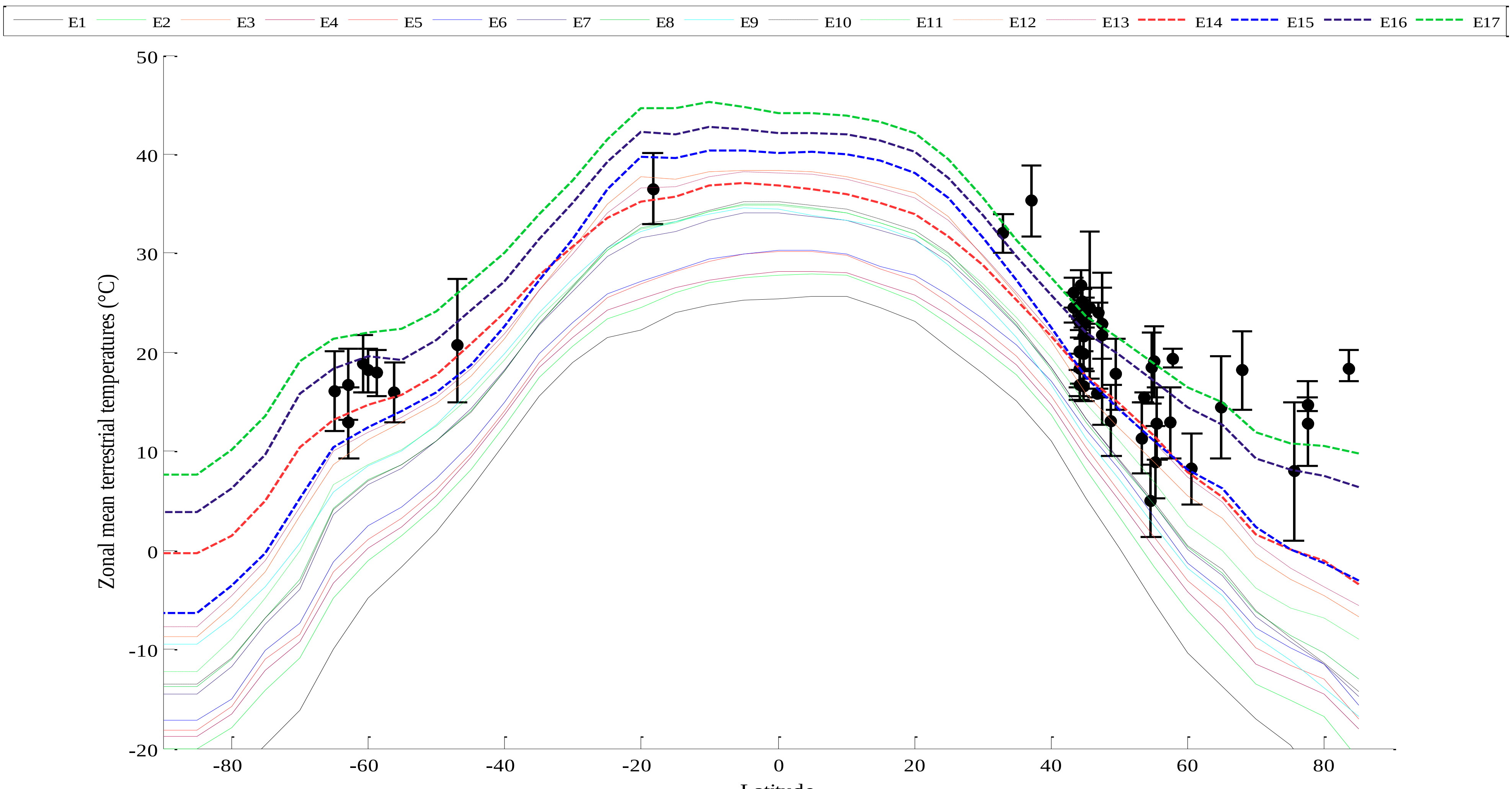
E1
E2
E3
E4
E5
E6
E7
E8
E9
E10
E11
E12
E13
E14
E15
E16
E17
Zonal mean terrestrial temperatures (°C)
50
40
30
20
10
0
-10
-20
-80
-60
-40
-20
0
20
40
60
80
Latitude

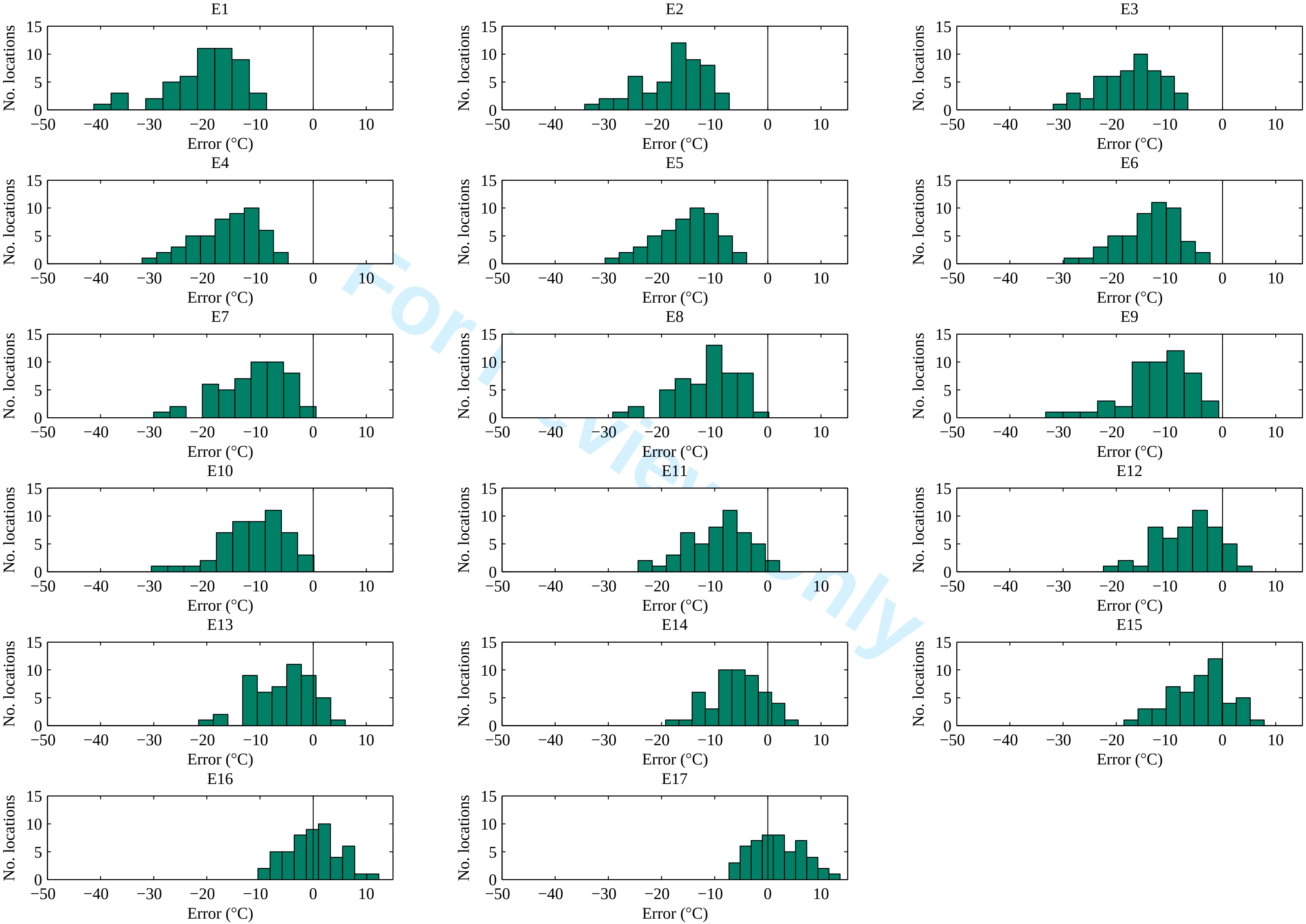
E1
E2
E3
E4
E5
E6
E7
E8
E9
E10
E11
E12
E13
E14
E15
E16
E17
No. locations
Error (°C)

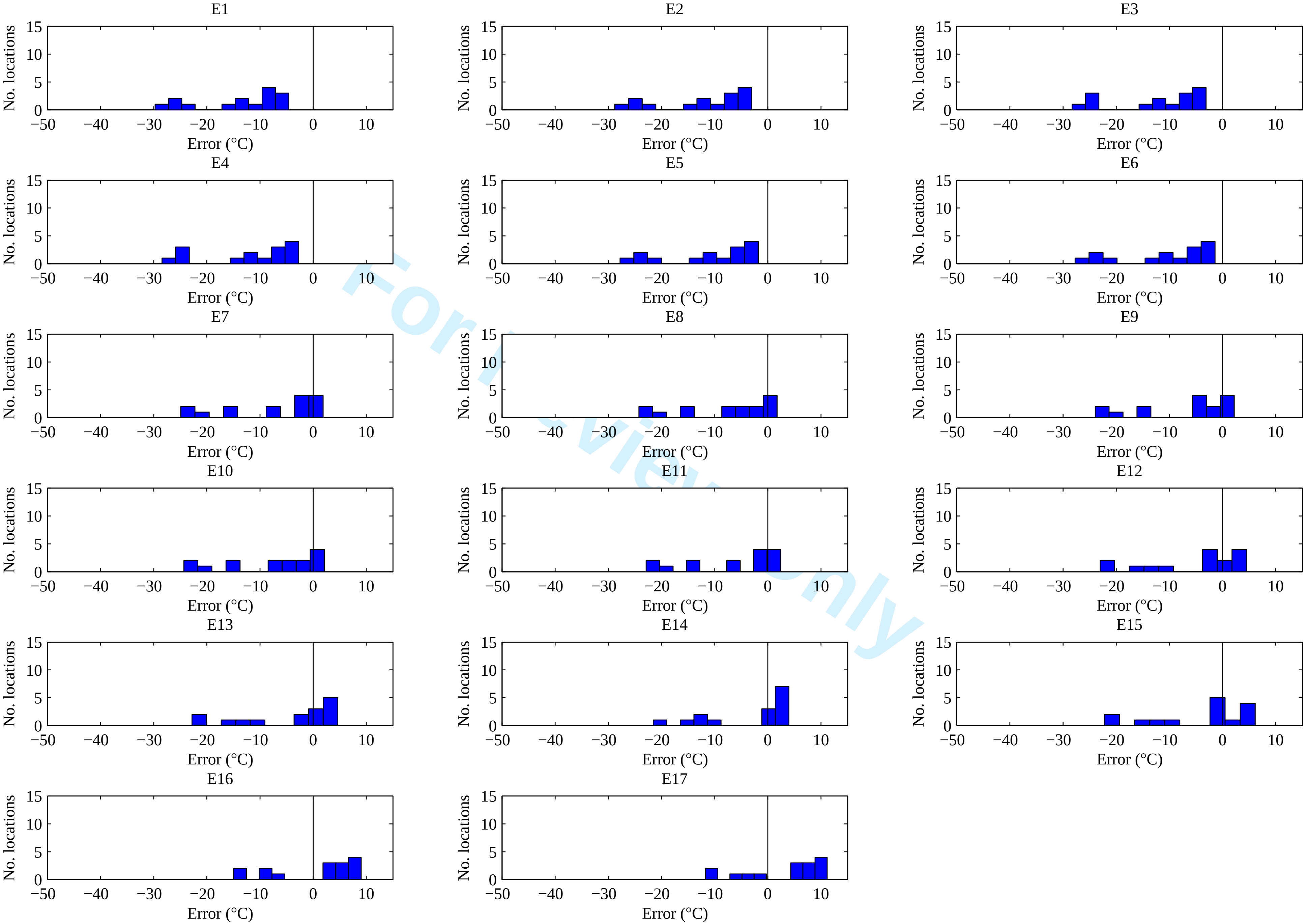
E1
E2
E3
E4
E5
E6
E7
E8
E9
E10
E11
E12
E13
E14
E15
E16
E17
No. locations
Error (°C)
15
10
5
0
−50
−40
−30
−20
−10
0
10

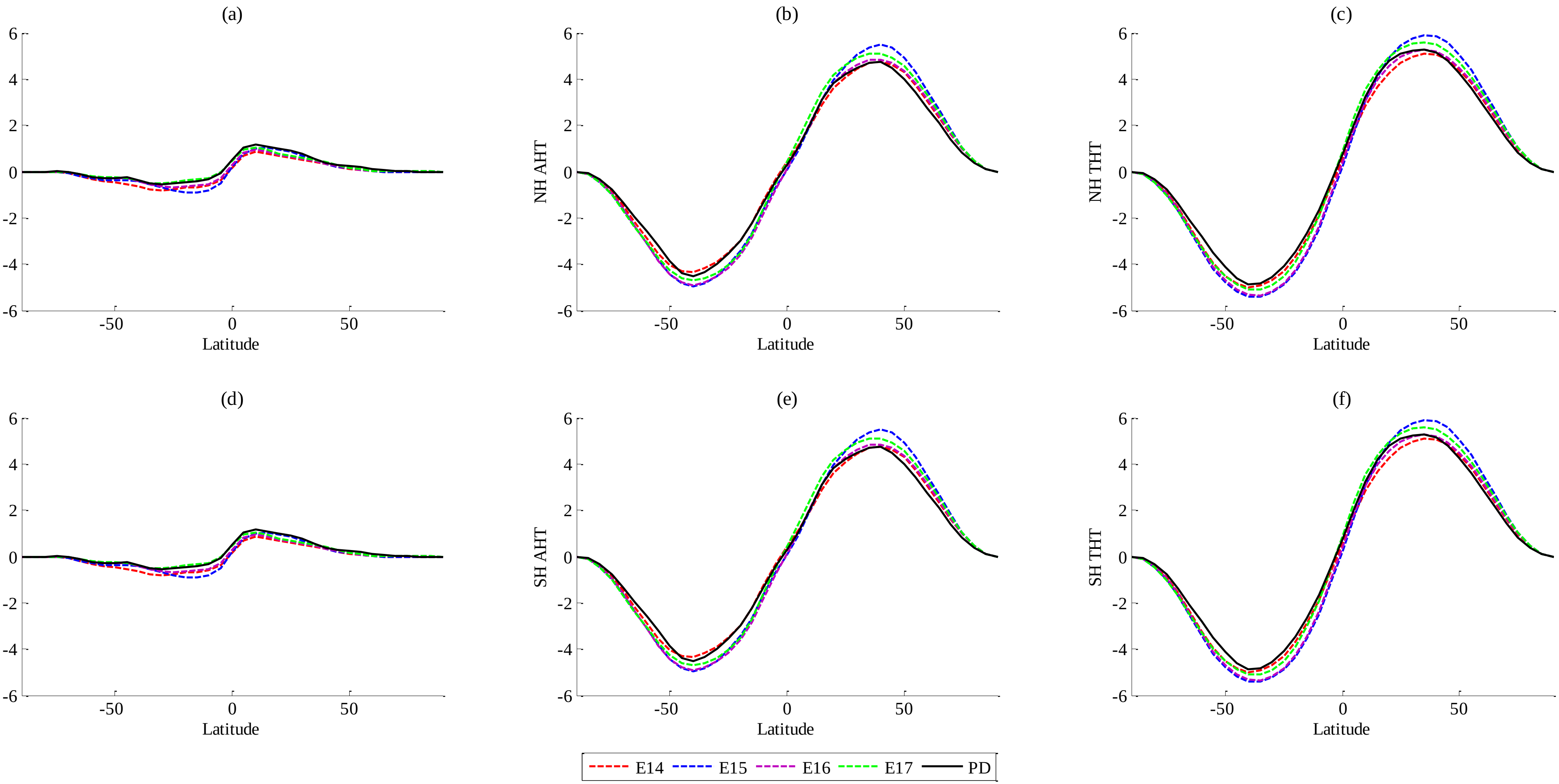
(a)
(b)
(c)
(d)
(e)
(f)
NH AHT
NH THT
SH AHT
SH THT
Latitude
-50
0
50
6
4
2
0
-2
-4
-6
E14
E15
E16
E17
PD

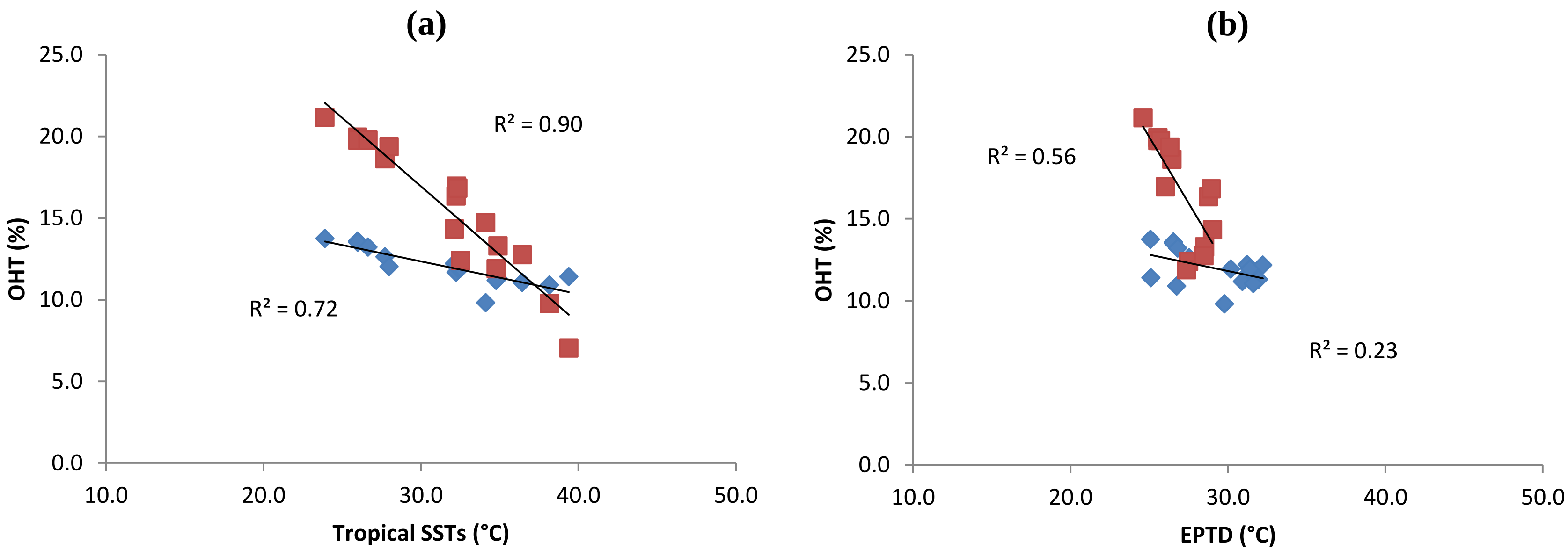
(a)
25.0
20.0
15.0
10.0
5.0
0.0
OHT (%)
R^2 = 0.90
R^2 = 0.72
10.0
20.0
30.0
40.0
50.0
Tropical SSTs (°C)
(b)
25.0
20.0
15.0
10.0
5.0
0.0
OHT (%)
R^2 = 0.56
R^2 = 0.23
10.0
20.0
30.0
40.0
50.0
EPTD (°C)